Molecular Cell, Volume *69*

Supplemental Information

Cand1-Mediated Adaptive Exchange Mechanism Enables Variation in F-Box Protein Expression

Xing Liu, Justin M. Reitsma, Jennifer L. Mamrosh, Yaru Zhang, Ronny Straube, and Raymond J. Deshaies

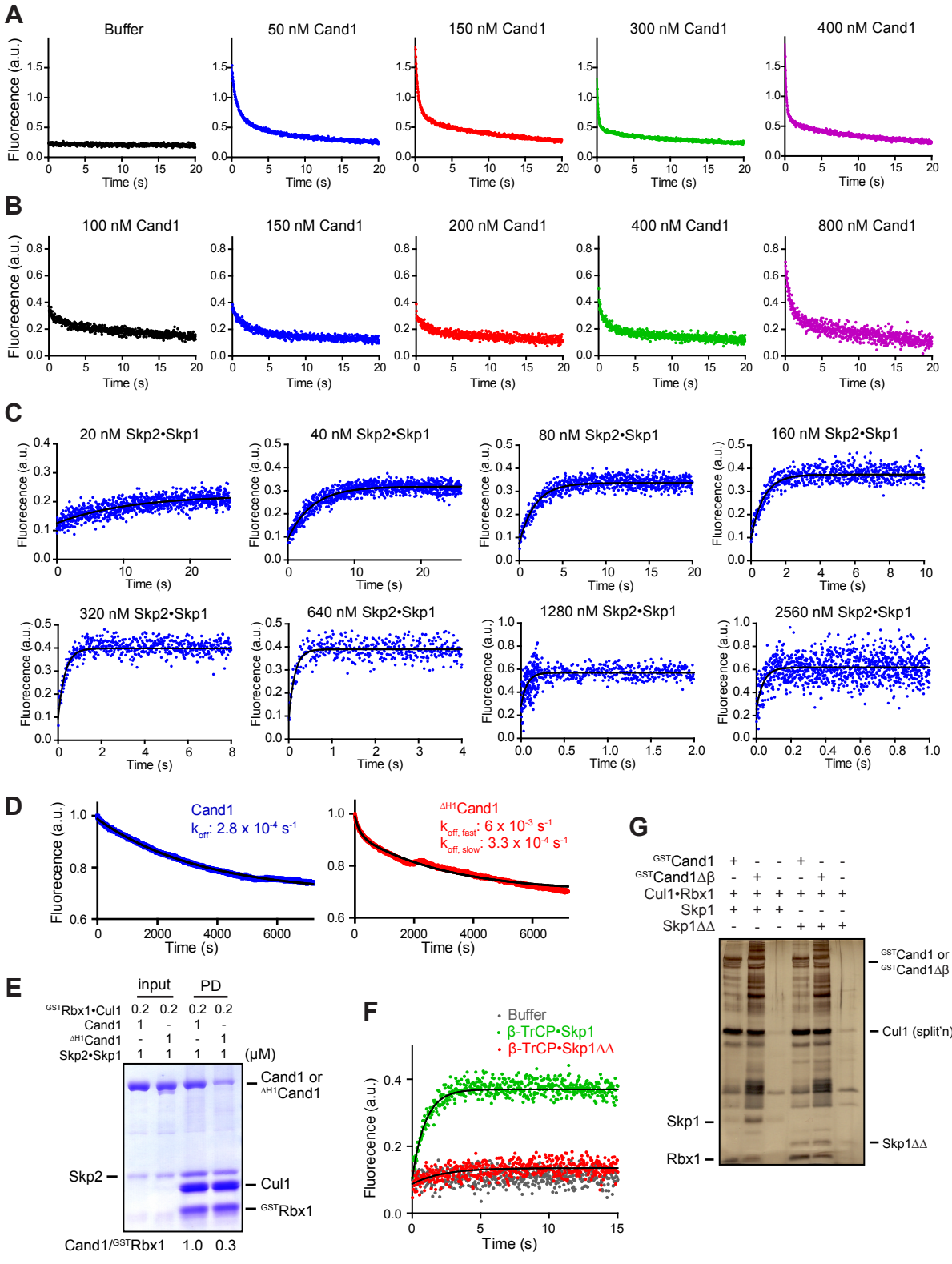
A
Buffer
50 nM Cand1
150 nM Cand1
300 nM Cand1
400 nM Cand1
Fluorescence (a.u.)
Time (s)
B
100 nM Cand1
150 nM Cand1
200 nM Cand1
400 nM Cand1
800 nM Cand1
C
20 nM Skp2•Skp1
40 nM Skp2•Skp1
80 nM Skp2•Skp1
160 nM Skp2•Skp1
320 nM Skp2•Skp1
640 nM Skp2•Skp1
1280 nM Skp2•Skp1
2560 nM Skp2•Skp1
D
Cand1
k_off: 2.8 x 10^-4 s^-1
ΔH1Cand1
k_off, fast: 6 x 10^-3 s^-1
k_off, slow: 3.3 x 10^-4 s^-1
E
input
PD
GSTRbx1•Cul1
Cand1
ΔH1Cand1
Skp2•Skp1
(μM)
Cand1 or ΔH1Cand1
Skp2
Cul1
GSTRbx1
Cand1/GSTRbx1 1.0 0.3
F
Buffer
β-TrCP•Skp1
β-TrCP•Skp1ΔΔ
G
GSTCand1
GSTCand1Δβ
Cul1•Rbx1
Skp1
Skp1ΔΔ
GSTCand1 or GSTCand1Δβ
Cul1 (split'n)
Skp1
Rbx1
Skp1ΔΔ

Figure S1

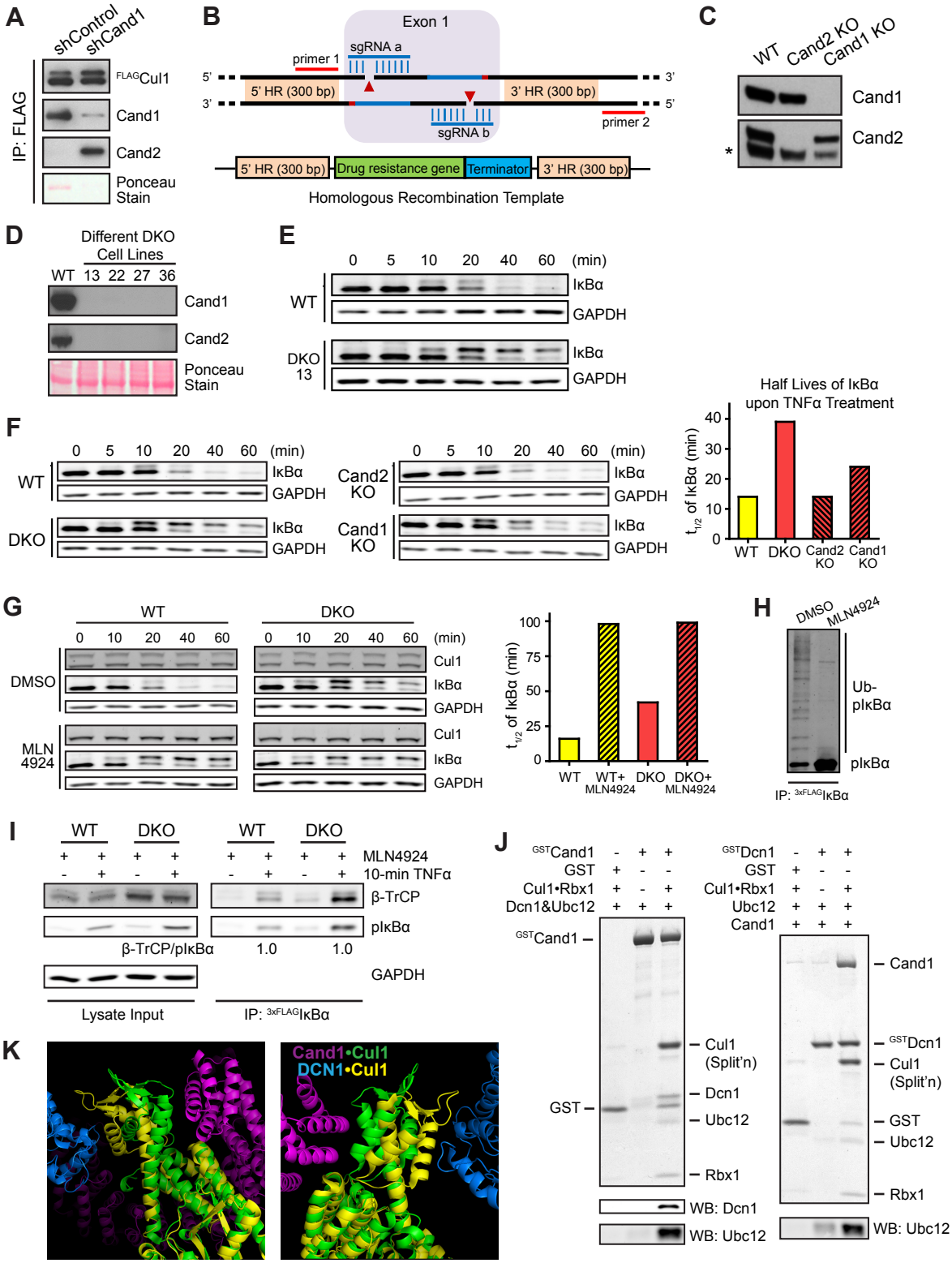
A
shControl
shCand1
IP: FLAG
FLAGCul1
Cand1
Cand2
Ponceau Stain
B
Exon 1
sgRNA a
primer 1
5'
3'
5' HR (300 bp)
3' HR (300 bp)
sgRNA b
primer 2
5' HR (300 bp)
Drug resistance gene
Terminator
3' HR (300 bp)
Homologous Recombination Template
C
WT
Cand2 KO
Cand1 KO
Cand1
Cand2
*
D
Different DKO Cell Lines
WT 13 22 27 36
Cand1
Cand2
Ponceau Stain
E
0 5 10 20 40 60 (min)
WT
DKO 13
IκBα
GAPDH
F
WT
DKO
Cand2 KO
Cand1 KO
IκBα
GAPDH
Half Lives of IκBα upon TNFα Treatment
t1/2 of IκBα (min)
WT DKO Cand2 KO Cand1 KO
G
WT
DKO
0 10 20 40 60 (min)
DMSO
MLN 4924
Cul1
IκBα
GAPDH
t1/2 of IκBα (min)
WT WT+ MLN4924 DKO DKO+ MLN4924
H
DMSO
MLN4924
Ub-pIκBα
pIκBα
IP: 3xFLAGIκBα
I
WT DKO WT DKO
MLN4924
10-min TNFα
β-TrCP
pIκBα
β-TrCP/pIκBα
1.0 1.0
GAPDH
Lysate Input
IP: 3xFLAGIκBα
J
GSTCand1
GST
Cul1•Rbx1
Dcn1&Ubc12
GSTDcn1
Ubc12
Cand1
Cand1
GSTDcn1
Cul1 (Split'n)
Dcn1
Ubc12
Rbx1
GST
WB: Dcn1
WB: Ubc12
K
Cand1•Cul1
DCN1•Cul1

Figure S2

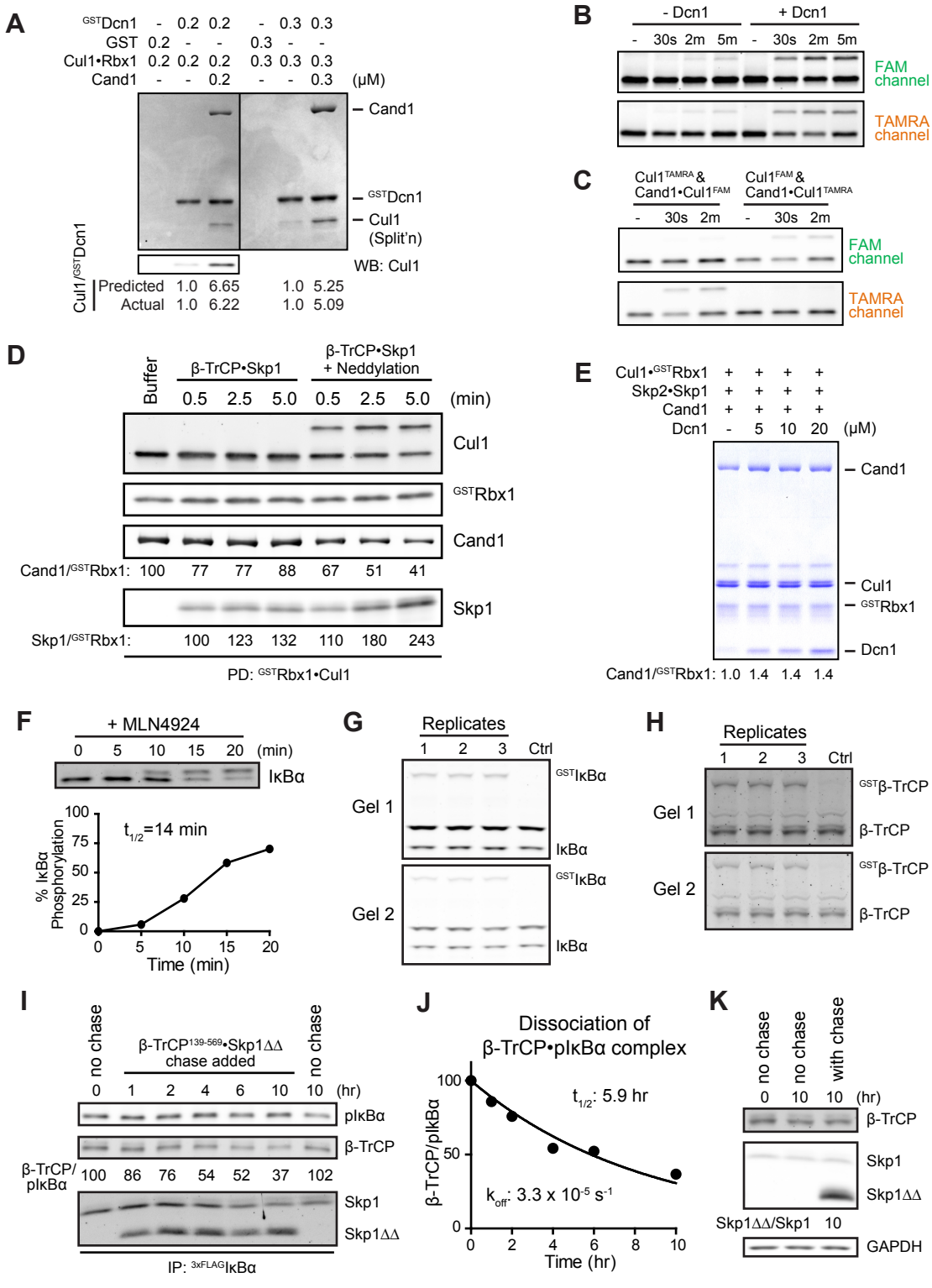
A
GSTDcn1 - 0.2 0.2 - 0.3 0.3
GST 0.2 - - 0.3 - -
Cul1•Rbx1 0.2 0.2 0.2 0.3 0.3 0.3
Cand1 - - 0.2 - - 0.3 (μM)
Cand1
GSTDcn1
Cul1 (Split'n)
WB: Cul1
Cul1/GSTDcn1
Predicted 1.0 6.65 1.0 5.25
Actual 1.0 6.22 1.0 5.09
B
- Dcn1
+ Dcn1
- 30s 2m 5m - 30s 2m 5m
FAM channel
TAMRA channel
C
Cul1TAMRA & Cand1•Cul1FAM
Cul1FAM & Cand1•Cul1TAMRA
- 30s 2m - 30s 2m
FAM channel
TAMRA channel
D
Buffer
β-TrCP•Skp1
β-TrCP•Skp1 + Neddylation
0.5 2.5 5.0 0.5 2.5 5.0 (min)
Cul1
GSTRbx1
Cand1
Cand1/GSTRbx1: 100 77 77 88 67 51 41
Skp1
Skp1/GSTRbx1: 100 123 132 110 180 243
PD: GSTRbx1•Cul1
E
Cul1•GSTRbx1 + + + +
Skp2•Skp1 + + + +
Cand1 + + + +
Dcn1 - 5 10 20 (μM)
Cand1
Cul1
GSTRbx1
Dcn1
Cand1/GSTRbx1: 1.0 1.4 1.4 1.4
F
+ MLN4924
0 5 10 15 20 (min)
IκBα
% IκBα Phosphorylation
t1/2=14 min
Time (min)
G
Replicates
1 2 3 Ctrl
Gel 1
Gel 2
GSTIκBα
IκBα
H
Replicates
1 2 3 Ctrl
Gel 1
Gel 2
GSTβ-TrCP
β-TrCP
I
no chase
β-TrCP139-569•Skp1ΔΔ chase added
no chase
0 1 2 4 6 10 10 (hr)
pIκBα
β-TrCP
β-TrCP/pIκBα 100 86 76 54 52 37 102
Skp1
Skp1ΔΔ
IP: 3xFLAGIκBα
J
Dissociation of β-TrCP•pIκBα complex
t1/2: 5.9 hr
koff: 3.3 x 10-5 s-1
β-TrCP/pIκBα
Time (hr)
K
no chase
no chase
with chase
0 10 10 (hr)
β-TrCP
Skp1
Skp1ΔΔ
Skp1ΔΔ/Skp1 10
GAPDH

Figure S3

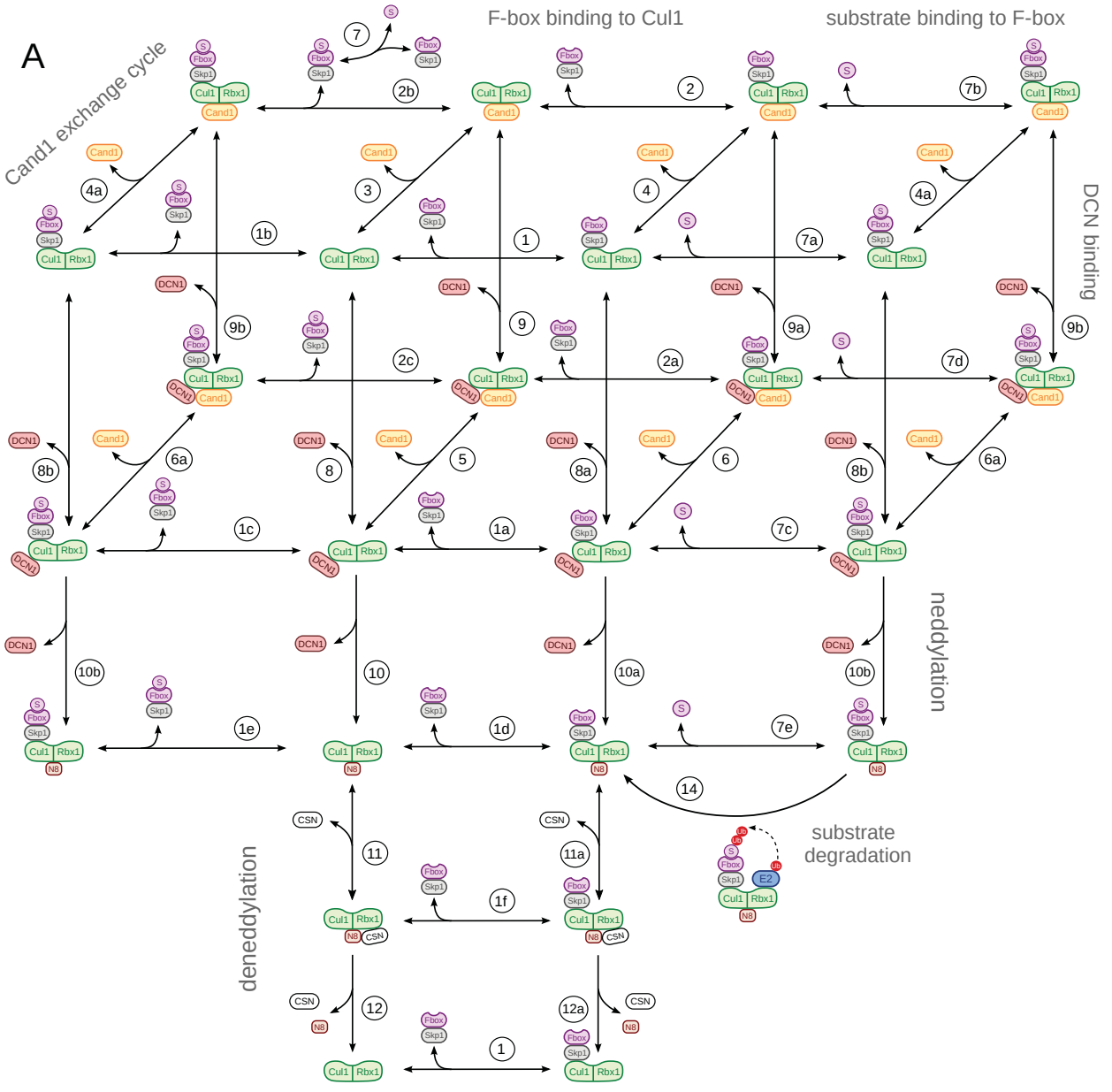
A
Cand1 exchange cycle
F-box binding to Cul1
substrate binding to F-box
DCN binding
neddylation
deneddylation
substrate degradation
B
product inhibition by CSN
C
detailed balance relations
$K_5 = \alpha K_3$
$K_9 = \alpha K_8$
K_8
K_3
K_1
$K_2 = \tau K_1$
$K_4 = \tau K_3$

Figure S4

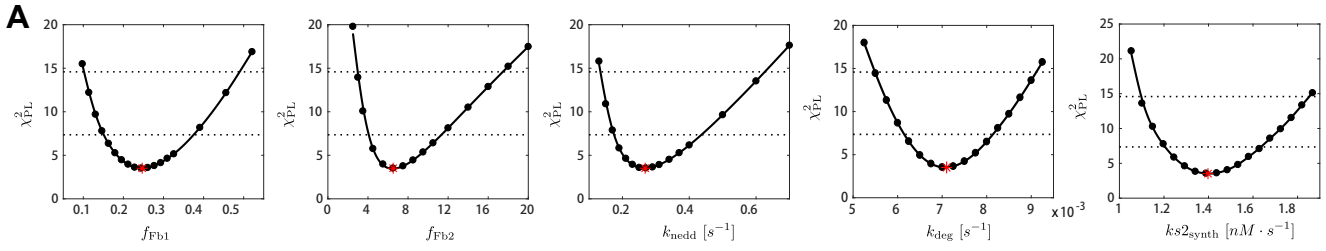

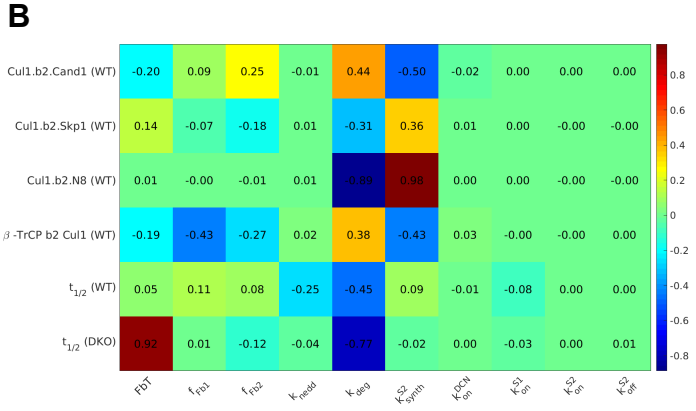

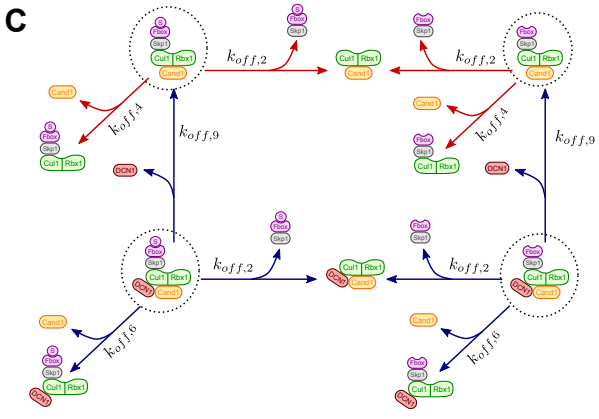

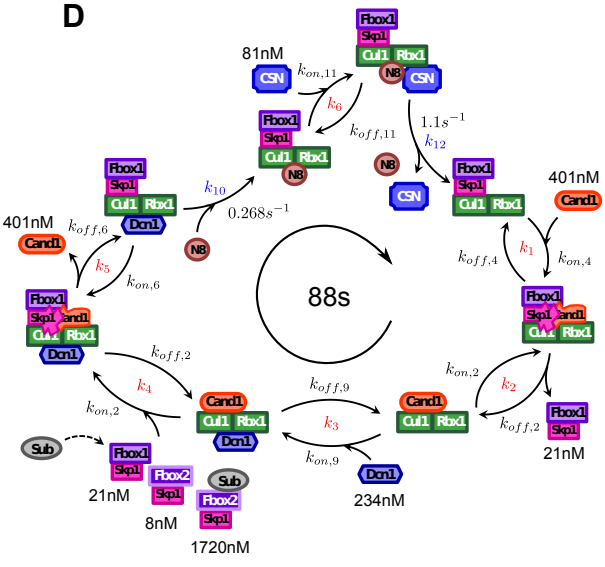

$(nM \cdot s)^{-1}$		s^{-1}		s^{-1}	
$k_{on,2}$	0.002	$k_{off,2}$	1.3	k_1	0.2
$k_{on,4}$	0.002	$k_{off,4}$	2.9	k_2	0.96
$k_{on,6}$	0.002	$k_{off,6}$	0.08	k_3	0.12
$k_{on,9}$	0.001	$k_{off,9}$	0.05	k_4	0.05
$k_{on,11}$	0.02	$k_{off,11}$	0.032	k_5	0.02
				k_6	1.57

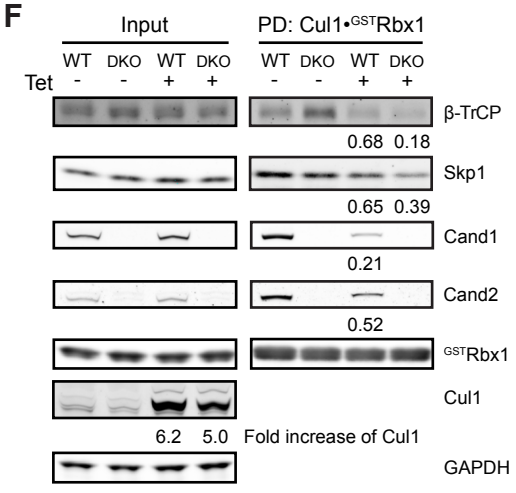

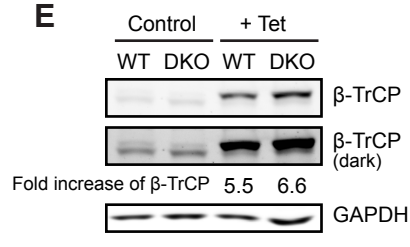

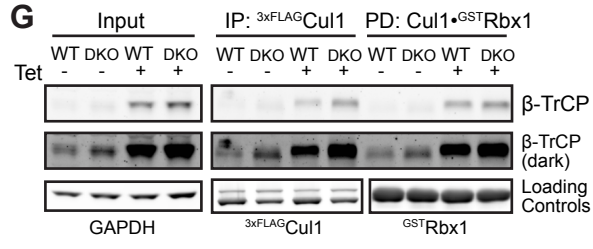

Figure S5

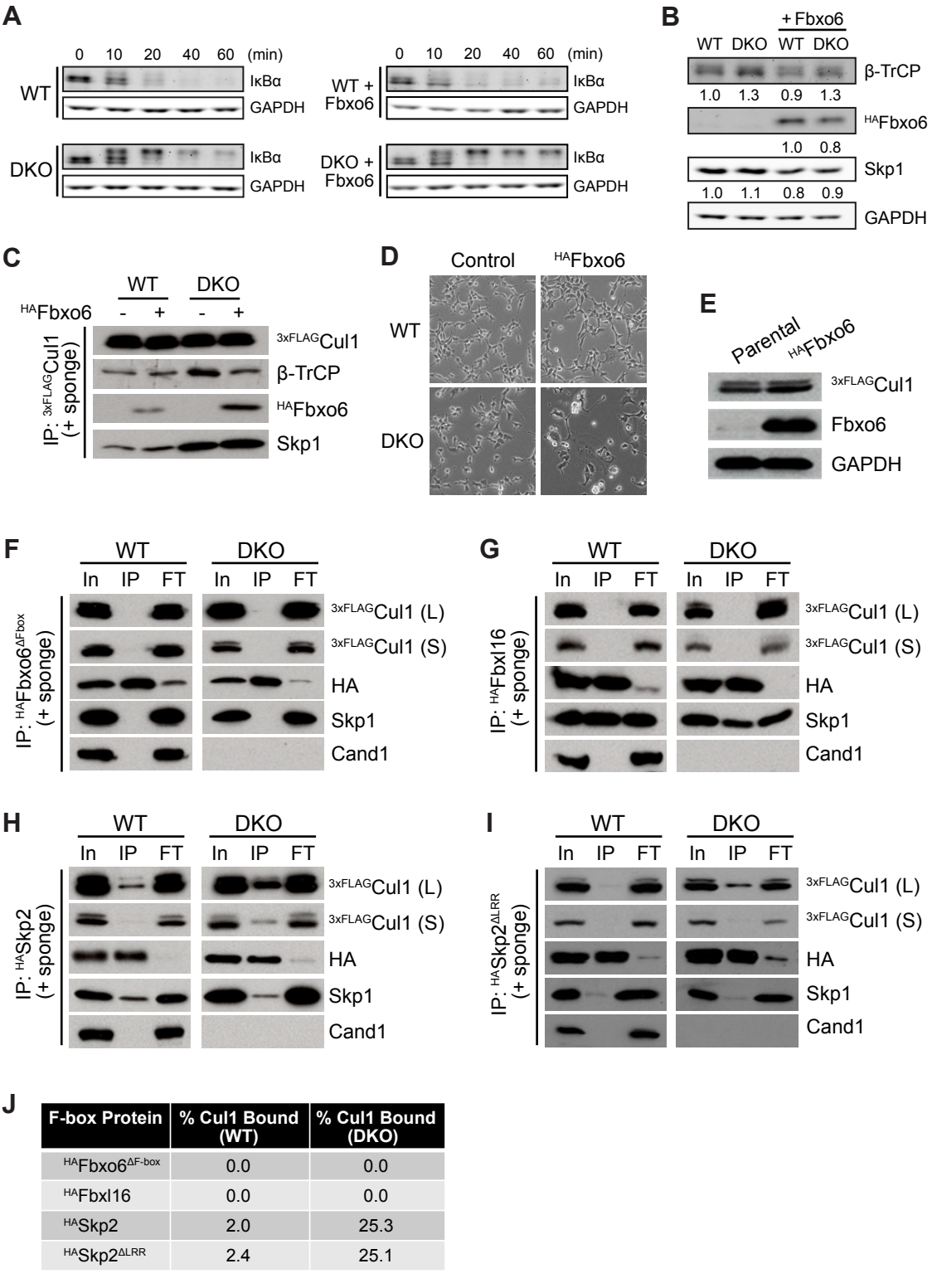

J

F-box Protein	% Cul1 Bound (WT)	% Cul1 Bound (DKO)
^{HA}Fbxo6$^{\Delta F\text{-box}}$	0.0	0.0
^{HA}Fbxl16	0.0	0.0
^{HA}Skp2	2.0	25.3
^{HA}Skp2$^{\Delta LRR}$	2.4	25.1

Figure S6

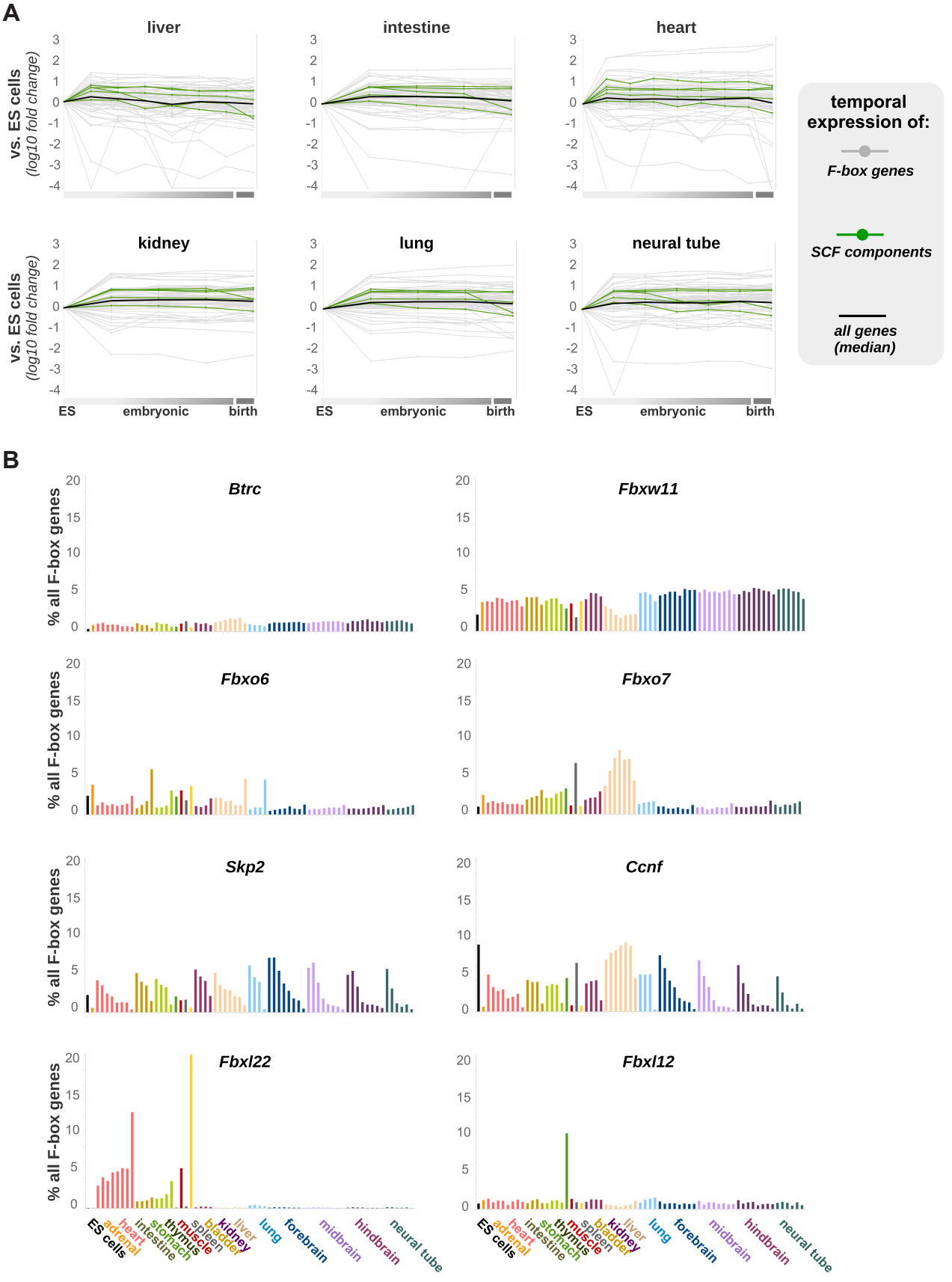
A
liver
intestine
heart
kidney
lung
neural tube
vs. ES cells
(log10 fold change)
ES
embryonic
birth
temporal expression of:
F-box genes
SCF components
all genes (median)
B
Btrc
Fbxw11
Fbxo6
Fbxo7
Skp2
Ccnf
Fbxl22
Fbxl12
% all F-box genes
ES cells
adrenal
heart
intestine
stomach
thymus
muscle
spleen
bladder
kidney
liver
lung
forebrain
midbrain
hindbrain
neural tube

Figure S7

SUPPLEMENTAL FIGURE LEGENDS

Figure S1. Properties of Cul1•Cand1 complex assembly and disassembly (related to Figure 1).

(A) k_{obs} for Cand1 binding to Cul1. The change in donor fluorescence versus time was measured in a stopped-flow fluorimeter upon addition of varying concentrations of $^{FlAsH\Delta H1}$Cand1 to 50 nM Cul1^{AMC}•Rbx1. Indicated concentrations are after 1:1 (v:v) mixing of the two solutions in the stopped-flow fluorimeter. Signal changes were fit to two phase exponential curves, and the fast-phase rates were used as k_{obs}. These values are plotted against [Cand1] in Fig 1B.

(B) k_{obs} for Cand1 binding to Cul1 preassembled with Skp1•Skp2. Similar to Fig S1A, except 100 nM Skp1•Skp2 was preincubated with 50 nM Cul1^{AMC}. Signal changes were fit to two phase exponential curves, and the fast-phase rates were used as k_{obs}. These values are plotted against [Cand1] in Fig 1C.

(C) k_{obs} for Cand1•Cul1 dissociation by Skp1•Skp2. The change in donor fluorescence versus time was measured in a stopped-flow fluorimeter upon addition of varying concentrations of Skp1•Skp2 to 10 nM $^{FlAsH\Delta H1}$Cand1•Cul1^{AMC}•Rbx1. Indicated concentrations are after 1:1 (v:v) mixing of the two solutions in the stopped-flow fluorimeter. Signal changes were fit to single exponential curves. These values are plotted against [Skp1•Skp2] in Fig 1E.

(D) Replacing the first helix of Cand1 with the tetracysteine tag increased the k_{off} of Cand1 from Cul1•Rbx1. Fluorescence emission at 445 nm (donor emission) was detected every 2 seconds after the addition of 10 x excess $^{FlAsH\Delta H1}$Cand1 (acceptor protein) to Cul1^{AMC}•Rbx1 pre-incubated with unlabeled Cand1 or $^{\Delta H1}$Cand1. FRET was observed following spontaneous dissociation of non-fluorescent Cand1 from Cul1^{AMC}•Rbx1. Signal changes were fit to exponential curves with a fixed end point of 70% initial donor fluorescence. Cand1•Cul1^{AMC}•Rbx1 was fit to a one phase curve. $^{\Delta H1}$Cand1•Cul1^{AMC}•Rbx1 was fit to a two phase curve, with $k_{off,\ slow}$ similar to the k_{off} of Cand1•Cul1^{AMC}•Rbx1 and $k_{off,\ fast}$ about 20 times faster.

(E) $^{\Delta H1}$Cand1•Cul1•Rbx1 is less stable than Cand1•Cul1•Rbx1. Skp1•Skp2, Cul1•^{GST}Rbx1, Cand1 or $^{\Delta H1}$Cand1 at indicated concentrations were used in the GST pulldown (PD) assay. Relative level of recovered Cand1 is shown as Cand1:^{GST}Rbx1 ratio. Based on this result and the known K_D of Cul1•Skp1•Fbxw7, the K_D of $^{\Delta H1}$Cand1•Cul1 is simulated to be ~4.5 times higher than the K_D of Cand1•Cul1. In this and other experiments employing recombinant Cul1, it migrates faster than expected because it is expressed by the 'split-n-coexpress' (split'n) method of Li et al (2005).

(F) β-TrCP removes Cand1 from Cul1 when it is in complex with full length Skp1 but not Skp1 with loop regions deleted. The change in donor fluorescence versus time was measured in a

stopped-flow apparatus upon addition of 75 nM Skp1•β-TrCP or Skp1ΔΔ•β-TrCP to 25 nM $^{FlAsH\Delta H1}$Cand1•Cul1^{AMC}•Rbx1.

(G) Deletion of β-hairpin in Cand1 or loop regions in Skp1 enables formation of a stable complex comprising Cul1, Skp1, and Cand1. *In vitro* pull-down assays containing the indicated proteins were performed to demonstrate the formation of stable complexes consisting of Cul1•Rbx1, Skp1 and ^{GST}Cand1 when Cand1 and/or Skp1 was mutated to delete structural elements that are predicted to clash in the Cand1•Cul1•Rbx1•Skp1 complex. The indicated proteins were mixed in equimolar amounts and bound to glutathione-4B resin. Proteins associated with the resin were fractionated by SDS-PAGE and detected by silver stain.

Figure S2. Degradation defects in Cand1Δ, Cand2Δ, and Cand1/2 double knockout cells (related to Figure 2). Complex of Cand1•Cul1•Dcn1 (related to Figure 3).

(A) Cand2•Cul1 complex was detected only when Cand1 was depleted. IP-WB analysis of Cand1•Cul1 and Cand2•Cul1 complexes in control (shControl) and Cand1 knock-down (shCand1) cells that are stably expressing the shRNA (Pierce et. al., 2013). Cells were treated with 1 μg/ml tetracycline for 1 hour 24 hours before collection to induce expression of ^{FLAG}Cul1 integrated at the FRT site (Flp-In system).

(B) Strategy for construction of Cand1/2 knockout cell lines. A pair of chimeric single-guide RNAs (sgRNA) guiding CRISPR Cas9 (D10A) nickases were designed to target the first exon of the Cand1 or Cand2 gene for mutagenesis. A homologous recombination (HR) template containing a drug resistance gene plus a translational terminator and two 300-bp homology arms that were identical to the genomic sequences flanking the first exon is depicted. Primer 1 and primer 2 were used to generate PCR products of the mutated genomic region for sequencing and confirming the complete inactivation of Cand1 and Cand2 genes. Note that primer 2 probed the region outside of the 300-bp HR region on the genomic DNA.

(C) Confirmation of Cand1 and Cand2 single KO cell lines. WB analysis showing the loss of Cand1 or Cand2 proteins in the corresponding KO cell lines. * marks a non-specific band, which serves as a loading control.

(D) Confirmation of Cand1/2 DKO cell lines. WB analysis showing the loss of Cand1 and Cand2 proteins in four DKO cell lines. DKO13, 22, 36 are independent cell lines confirmed by sequencing results. The filter stained with Ponceau S prior to probing is shown as a loading control. These lines initially displayed slower growth than the wild type (WT) cells, but the growth rate gradually increased after a few passages and became similar to the WT cells by the time their genotypes were confirmed.

(E) IκBα degradation is defective in DKO13 cells. WB analysis of IκBα levels in WT and DKO13 cells at indicated time points after TNFα treatment. DKO13 shows an IκBα degradation defect similar to the DKO22 and DKO36 lines shown in Fig 2A.
(F) Cand1 but not Cand2 is required for proper degradation of IκBα. WB analysis of IκBα degradation in response to TNFα treatment in WT, Cand1/2 DKO, Cand2 single knockout (Cand2 KO) and Cand1 KO cells. Half-lives of IκBα in this analysis are shown in the graph.
(G) Inhibiting neddylation stabilizes IκBα in both WT and DKO cells and enables quantification of the rate of IκBα phosphorylation. WB analysis of IκBα degradation in response to TNFα treatment in WT and DKO cells pretreated with either 0.1% DMSO or 1 μM MLN4924 for 1 hr. Half-lives of IκBα in this analysis are shown in the graph.
(H) Inhibiting neddylation strongly inhibits IκBα ubiquitination. Expression of ^{3xFLAG}IκBα cDNA integrated at the FRT site was induced with tetracycline for 24 hours and then ^{3xFLAG}IκBα was immunopreciptiated from cell lysate with anti-FLAG following pre-treatment of the cells with either 0.1% DMSO or 1 μM MLN4924 for 1 hr before 10-min TNFα treatment. IPs were evaluated by WB analysis with antibodies against pIκBα.
(I) pIκBα binds β-TrCP with equal efficiency in WT and DKO cells. WT and DKO cells expressing tetracycline-induced ^{3xFLAG}IκBα and treated with 1 μM MLN4924 for 1 hr to block pIκBα ubiquitination were lysed and subjected to IP with anti-FLAG followed by WB analysis with the indicated antibodies to evaluate interaction between pIκBα and β-TrCP. This is essentially the same as the experiment in Fig 2G, except that ubiquitination of pIκBα was suppressed by MLN4924, instead of by treating the IPs with deububiquitinating enzyme Usp2. MLN4924 or Usp2 were used to collapse all pIκBα species into a single band to facilitate quantification.
(J) Cand1 forms a complex with Dcn1 and Ubc12 only in the presence of Cul1. Reciprocal pull-down assays were set up as indicated. Each protein was included at 1 μM. Proteins adsorbed to the glutathione beads were fractionated by SDS-PAGE and stained by Coomassie blue or subjected to WB with the indicated antibodies.
(K) Binding of Cand1 alters the conformation of the Dcn1 binding site on Cul1. The C-terminal domains of Cul1 from PDB files of “4P5O” and “1U6G” were aligned in PyMOL, and the front and back views of the aligned Cand1•Cul1•Dcn1 are shown. Cand1 is in magenta and Dcn1 is in blue; Cul1 in complex with Cand1 is in green, and Cul1 in complex with Dcn1 is in yellow.

Figure S3. Cand1 and neddylation (related to Figure 3). Development of the computational model (related to Figure 4 and Method S1).

(A) Confirmation of the estimated K_D of 5 x 10^{-8} M for Dcn1 binding to Cand1•Cul1•Rbx1. Assays were similar to Fig 3C but lower concentrations of Cul1, Cand1 and ^{GST}Dcn1 were used. Proteins adsorbed to the glutathione beads were fractionated by SDS-PAGE and stained by Coomassie blue or subjected to WB with the Cul1 antibody. Fold increase of Cul1 recovered from the pulldown assay calculated by the K_D values (Predicted) and measured from the experiments (Actual) are shown.

(B-C) Negative controls for Fig 3F. (B) A mixture of 0.2 μM Cul1^{FAM} and 0.2 μM Cul1^{TAMRA} with or without 0.2 μM Dcn1 was incubated with 0.1 μM each of Nedd8, Ubc12, and NAE for indicated time period. FAM and TAMRA signals were detected by a Typhoon scanner.

(C) 5x Skp1•Skp2 and DKO lysate indicated in Fig 3E was replaced with 0.1 μM each of Nedd8, Ubc12, and NAE, and no FBP was added.

(D) Neddylation promotes the formation of SCF during the exchange process. Cand1, Dcn1 and Cul1•^{GST}Rbx1 were pre-incubated with glutathione beads and then mixed 1:1 (v:v) with protein solution containing Skp1•β-TrCP and Ubc12 or Ubc12~Nedd8. At indicated time points after mixing, beads were washed and eluted, and immobilized proteins were fractionated by SDS-PAGE and detected by WB. Final concentrations of the protein components were the same as in Fig 3G.

(E) Dcn1 stabilizes the Cand1•Cul1•Rbx1 complex in the presence of FBP. Pulldown analysis of recombinant Cand1 (1 μM) bound to recombinant Cul1•^{GST}Rbx1 (0.5 μM) in the presence of Skp1•Skp2 (2 μM) and increasing concentrations of Dcn1 (0-20 μM). Protein samples were fractionated by SDS-PAGE and stained with Coomassie Blue. Normalized levels of Cand1 recovered were calculated as the ratio of Cand1 to ^{GST}Rbx1.

(F) WB estimation of IκBα phosphorylation rate. WT cells were treated with 1 μM MLN4924 for 1 hr to inhibit the ubiquitination and degradation of pIκBα, and then sampled at indicated time points after TNFα treatment. The $t_{1/2}$ of IκBα phosphorylation is estimated to be 14 min.

(G-H) Concentration of endogenous IκBα is 10 times higher than endogenous β-TrCP. WB quantification of the endogenous IκBα (G) and β-TrCP (H) concentrations in WT cells, with recombinant ^{GST}IκBα (G) and ^{GST}β-TrCP (H) spiked into cell lysate as the internal standards. Three biological replicates were analyzed on two individual gels as technical replicates. The concentration of IκBα was estimated to be 650 ± 66 nM (SD, n=6). The concentration of β-TrCP was estimated to be 64 ± 6 nM (SD, n=6). In other experiments, sample titration was performed to confirm that the band intensities measured here were within the linear range of the instrument.

(I-K) pIκBα and β-TrCP form a very stable complex in cells. IP-WB analysis of the dissociation rate of the pIκBα•β-TrCP complex in cell lysate is shown in (I). DKO cell lysate containing 3xFLAG tagged pIκBα with or without added recombinant Skp1ΔΔ•β-TrCP$^{139-569}$ chase protein (~100x of endogenous β-TrCP level) was incubated at room temperature for indicated times. Dissociation of β-TrCP from pIκBα was calculated as ratios of β-TrCP to pIκBα signals in anti-FLAG IPs, and these ratios were used to estimate k_{off} (J) based on a fit to a single exponential. Lysate input for (I) is shown in (K). The amount of recombinant Skp1ΔΔ•β-TrCP$^{139-569}$ chase protein added was in large excess of total endogenous Skp1•FBP complexes as judged by relative signals for Skp1 and Skp1ΔΔ. In addition, the level of endogenous β-TrCP in the lysate remained constant throughout a10-hr incubation at room temperature with or without added chase protein.

Figure S4. Detailed reaction scheme of the SCF cycle model (related to Figure 4 and Method S1).

(A) The scheme depicts the state variables and the reactions in the network as listed in Method S1 (Tables T2-T13). Fbox and S denote either Fb1 and S1 (relating to β-TrCP and pIκBα) or Fb2 and S2 (relating to auxiliary substrate receptors and their substrates). Lines with unidirectional arrows represent irreversible reactions. Reactions labeled by the same number (but different lower case letters) have the same kinetic parameters (Tables T3-T13 of Method S1). Note that for better visibility some states are drawn twice in the network.

(B) Reactions describing product inhibition of CSN by unneddylated Cul1 species. We assume that states in which Cul1 is not neddylated and its associated FBP is not bound to substrate, can bind CSN leading to the formation of complexes which are devoid of SCF ligase activity.

(C) Illustration of the detailed balance relations for the thermodynamic cycles involving Cand1 and FBP (lower cycle, $K_1K_4 = K_2K_3$), and Cand1 and Dcn1 (upper cycle , $K_8K_5 = K_3K_9$) (see Method S1 for details).

Figure S5. Parameter identifiability analysis, response matrix, computation of protein fractions and cycle time (related to Figure 4, Figure 7 and Method S1). Experimental tests of the mathematical model predictions (related to Figure 5).

(A) Profile likelihood as a function of estimated parameters (Table T15 of Method S1). Circles were determined by numerically computing the profile likelihood according to Eq. (S10). Red circles represent the optimal parameter values that minimize χ^2 as defined in Eq. (S9). Solid lines are smooth interpolations of the data points. Horizontal dotted lines represent thresholds

as defined in Eq. (S11) that were used to derive 95% confidence intervals, either pointwise (lower line) or simultaneous (upper line).

(B) Matrix of response coefficients as defined by Eq. (S12) (see Method S1). Parameters on the horizontal axis were increased by 10% and the relative change of different observable quantities (vertical axis) was computed. Positive / negative response coefficients indicate a positive / negative correlation between parameter and observable quantity. Absolute values larger (smaller) than 1 indicate a high (low) sensitivity with respect to the corresponding parameter. The greater the absolute value of a response coefficient, the more sensitive the respective quantity is to changes in the corresponding parameter. Parameters are defined in Table T15 of Method S1. The abbreviation “b2“ means “bound to“.

(C) The scheme illustrates the computation of the coefficients defined in Eqs. (S13) and (S14) which determine the contribution of the encircled protein complexes to the protein fractions Cand1.b2.Cul1 and Skp1.b2.Cul1 as defined in Table T14 of Method S1. Note that these complexes are unstable (since they contain both Cand1 and FBP), and thus cannot be detected in our pull-down assays. Fb and S may denote Fb1 (β-TrCP) and S1 or Fb2 (auxiliary SRs) and S2.

(D) Illustration of the computation of the cycle time according to Eq. (S21). Concentrations represent steady state concentrations of free (unbound) proteins obtained from simulations using parameters for WT cells (Table T2-T13, T15 of Method S1). Numbers in the table summarize the values of the on and off rate constants as well as the corresponding net rate constants (red color) computed from Eqs. (S15) - (S20).

(E) Confirmation of β-TrCP overproduction in Fig 5C by WB analysis. Fold increase in total β-TrCP levels are indicated. (dark): more intense exposure of β-TrCP blot. A 9-fold increase in total β-TrCP level in both WT and DKO cells was observed in a replicate experiment.

(F) Overexpression of ^{3xFLAG}Cul1 reduces levels of unassembled cellular β-TrCP, Cand1 and Cand2. As depicted in Fig 5D, WT and DKO cells were treated with or without tetracycline to induce expression of a stably integrated ^{3xFLAG}Cul1 transgene, and then lysed in the presence of excess Cul1•^{GST}Rbx1 to capture unassembled β-TrCP, Skp1, Cand1, and Cand2. Lysates were subjected to pulldown with glutathione beads, and bound fractions were subjected to WB with the indicated antibodies. One set of representative results from two replicate experiments are shown. These are the underlying data for the graph in Fig 5E.

(G) Overproduction of β-TrCP modestly reduces the efficiency of its assembly with Cul1. As depicted in Fig 5F, WT and DKO cells with 3xFLAG-tagged endogenous Cul1 were treated with or without tetracycline to induce expression of a stably integrated β-TrCP transgene, and then

lysed in the presence of excess Cul1•^{GST}Rbx1 to suppress Cand1-mediated exchange and capture unassembled Skp1•β-TrCP complexes. Lysates were subjected to IP with anti-FLAG followed by pull-down with glutathione beads. Bound fractions were subjected to WB with the indicated antibodies. One set of representative results from two replicate experiments are shown. These are the underlying data for the graph in Fig 5G.

Figure S6. FBP-dependent sequestration of Cul1 inhibits proliferation of DKO cells (related to Figure 6).

(A-B) Fbxo6 overexpression further slows IκBα degradation rate in the DKO cells. These are the underlying data for the graph in Fig 6A. Cells were infected with lentiviruses to overproduce Fbxo6 and were subjected to TNFα treatment three days after the viral infection.

(B) WB analysis of β-TrCP, ^{HA}Fbxo6, and Skp1 in the cell lysates from panel (A). Relative protein levels are indicated below each blot.

(C) Overproduction of ^{HA}Fbxo6 decreases the endogenous SCF$^{β\text{-}TrCP}$. ^{3xFLAG}Cul1 was immunoprecipitated from WT and DKO cells overexpressing ^{HA}Fbxo6 in the presence of recombinant Cul1•^{GST}Rbx1 (+ sponge). Co-immunoprecipitated β-TrCP and ^{HA}Fbxo6 were analyzed by WB.

(D) Overexpression of Fbxo6 alters the morphology of DKO cells. Live cell images were acquired at 20x magnification seven days after viral infection.

(E) WB with anti-Fbxo6 antibody showing ^{HA}Fbxo6 overproduction five days after infection with recombinant lentivirus. The overproduction is estimated to be 45 times of the endogenous level.

(F-I) Co-IP of ^{3xFLAG}Cul1 with overexpressed ^{HA}Fbxo6^{ΔFbox} (F), ^{HA}Fbxl16 (G), ^{HA}Skp2 (H), and ^{HA}Skp2^{ΔLRR} (I) in the presence of recombinant Cul1•^{GST}Rbx1 (+ sponge). Cells were infected by lentiviruses to overexpress different FBPs, and the experimental procedures were similar to Fig 6D. Long (L) and short (S) exposures of endogenous ^{3xFLAG}Cul1 are shown.

(J) Quantification of the relative percent of Cul1 co-immunoprecipitated with overexpressed FBPs in (F-I), n = 2.

Figure S7. FBP expression is dynamic during mouse development (related to Figure 6 and Discussion).

(A) Expression of FBP genes is highly variable during development of multiple tissues, despite stable expression of core SCF components. RNA-seq data from ENCODE for the indicated tissues during mouse development were normalized to ES cell expression levels. Fold change for each embryonic and birth timepoint relative to ES cells is presented in log10 scale. Each

datapoint is derived from FPKM RNA-seq values and is the average of two replicates. Grey datapoints and lines represent expression of 73 FBPs, green represents SCF complex components (Cul1, Rbx1, Skp1, Cand1, and Cand2), and black represents the median fold change for all transcripts expressed in ES cells (25130 transcripts).
(B) Expression of many FBPs is highly dynamic during development. RNA-seq data from ENCODE for mouse development was obtained as FPKM values, and averaged for two replicates. For selected FBPs, expression levels relative to total expression of 73 FBPs was calculated for each tissue and timepoint. Distinct colors represent different tissues as listed on the bottom, and bars in the same color represent different embryonic developmental timepoints from early organogenesis (leftmost; timepoint varies by tissue) to birth (rightmost). Tissues with only one timepoint represent gene expression at birth.

METHOD S1: Mathematical model, related to Figure 4, Figure 7, Figure S4-S5

Protein concentrations (HEK293 cells)

Table T1

protein	**concentration [nM]**	**reference**
Cul1	522	Reitsma et al. 2017
Cand1	1210	
CSN [(a)]	378	
DCN1	325	
Skp1	2107	
Rbx1	1724	
Nedd8 (N8)	3373	
β-TrCP	64	this paper
IκBα	647	this paper

[(a)] average value of CSN1-CSN8 excluding CSN7

Total DCN concentration

In humans there are 5 DCN proteins (DCN1-5) all of which bind to Cul1 with similar affinity [Monda et al. (2013), Keuss et al. (2016)]. In addition, it seems that the 5 DCN proteins are partially functionally redundant so that the effective pool of catalytically active DCN proteins is likely to be larger than the DCN1 pool. To account for this effect in our model we defined the total DCN concentration by

$$[DCN] = f_{DCN1} \cdot [DCN1]. \tag{S1}$$

To estimate the scale factor f_{DCN1} we note that in HeLa cells the total copy number of DCN proteins (DCN1-5) amounts to 256892 of which the sum of DCN1 and DCN2 equals 94931 [Kulak et al., 2014]. Assuming that the concentrations of DCN1 and DCN2 are equal and that the relative proportions of DCN proteins in HEK 293 cells are similar to those in HeLa cells we obtain $f_{DCN1} = 256892/(94931/2) \approx 5.4$ which suggests that $5 \leq f_{DCN1} \leq 6$. In the simulations we used $f_{DCN1} = 6$.

Sequestration of Cand1, CSN and DCN1 by other cullins

Cand1, CSN and DCN1 do not only bind to Cul1 but also to other cullins (Cul2-Cul5) in cullin-RING ubiquitin ligases (CRLs) [Bennett et al., 2010] which reduces the amounts of Cand1, CSN and DCN1 that are available for binding to Cul1. To account for this effect in our model we defined effective Cand1, CSN and DCN1 concentrations through

$$[Cand1]_{eff} = f_{Cand1,WT} \cdot [Cand1] \tag{S2}$$

$$[DCN1]_{eff} = f_{DCN1,WT} \cdot [DCN] \tag{S3}$$

$$[CSN]_{eff} = f_{CSN,WT} \cdot [CSN] \tag{S4}$$

where $[Cand1]$, $[DCN]$ and $[CSN]$ are defined in Table T1 and Eq. (S1). Since DCN proteins bind cullins with similar affinity (within a factor of ~10) [Monda et al. (2013), Keuss et a. (2016)] we assumed that the scale factor $f_{DCN1,WT}$ is proportional to the relative abundance of Cul1, i.e.

$$f_{DCN1,WT} = \frac{[Cul1]}{[Rbx1] + [Cul5]} = \frac{522nM}{1724nM + 548nM} \approx 0.23. \quad \text{(S5)}$$

Here we used the concentration of Rbx1 (cf. Table T1) as a measure for the concentration of Cul1-Cul4 all of which form stable heterodimers with Rbx1 [Lydeard et al., 2013]. The concentration of Cul5 was extrapolated from the value reported in [Bennett et al., 2010] according to

$$[Cul5] = \frac{[Cul1]}{[Cul1]_{Bennett}}[Cul5]_{Bennett} \approx \frac{522nM}{302nM}317nM \approx 548nM.$$

For simplicity, we used the same scale factor for CSN as for DCN defined in Eq. (S5), i.e.

$$f_{CSN,WT} = f_{DCN1,WT} \approx 0.23. \quad \text{(S6)}$$

However, previous measurements have shown that if neddylation is inhibited the fraction of Cand1 associated with Cul1 is 0.4/0.75 ≈ 0.54 (Fig. S6 in [Bennett et al., 2010]) suggesting that more than half of the total Cand1 pool is associated with Cul1 under cellular conditions. Hence, we set $f_{Cand1,WT} = 0.54$ in Eq. (S2).

State variables and initial conditions

Table T2 lists the state variables together with their initial values as used in our simulations. F-box proteins (Fb) bind to Cul1 via the Skp1 adaptor protein. Due to the 1:1 stoichiometry between Skp1 and F-box proteins the total concentration of substrate receptors (Skp1•F-box dimers) is bounded by the availability of Skp1 proteins, i.e. [FbT] ≤ [Skp1] = 2107nM. In principle, it is conceivable that the amount of Skp1•F-box heterodimers is lower than the total amount of Skp1. However, to reduce the number of parameters that have to be estimated by comparing model simulations with experiments (cf. Parameter estimation) we set [FbT] = [Skp1].

Model reaction and rate constants

We modeled the CRL cycle as a mass-action network. The network states together with the elementary reactions are depicted in Figs. S4A and S4B. The state variables together with their default initial values are defined in Table T2. Reversible reactions were parametrized by k_{on} and k_{off} rate constants while irreversible reactions were parametrized by (pseudo) first-order rate constants. The latter may represent an effective k_{cat} (as for neddylation and deneddylation) or a specific degradation rate (as in the case of substrate degradation). Reactions with the same set of parameters are labelled by the same digit (1-16). Individual reactions within a group of reactions with the same set of parameters are distinguished by a lower case letter (a,b,c,…).

In our model we considered two sets of F-box proteins, β-TrCP (Fb1) and auxiliary (background) substrate receptors (Fb2). In Fig. S4A and S4B only reactions involving Fb1 are shown. For each reaction involving Fb1 or S1 there exists a corresponding reaction for Fb2 or S2 which is listed in the tables below without an explicit reaction number.

Table T2

state variable	IC[(a)]	state variable	IC	state variable	IC
Cul1[(b)]	522 nM	Cul1•Cand1	0	N8-Cul1•CSN	0
Cand1[(b)]	1210 nM	Cul1•Fb1	0	Cul1•DCN1•Fb1	0
DCN1[(b)]	325 nM	Cul1•Fb2	0	Cul1•DCN1•Fb2	0
CSN[(b)]	378 nM	Cul1•Fb1•S1	0	Cul1•DCN1•Fb1•S1	0
FbT[(c)]	2107 nM	Cul1•Fb2•S2	0	Cul1•DCN1•Fb2•S2	0
Fb1[(b,d)]	64 nM	Cul1•Cand1•Fb1	0	Cul1•Cand1•DCN1	0
Fb2[(e,f)]	2043 nM	Cul1•Cand1•Fb2	0	Cul1•Cand1•DCN1•Fb1	0
Fb1•S1	0	Cul1•Cand1•Fb1•S1	0	Cul1•Cand1•DCN1•Fb2	0
Fb2•S2	0	Cul1•Cand1•Fb2•S2	0	Cul1•Cand1•DCN1•Fb1•S1	0
N8-Cul1	0	N8-Cul1•Fb1	0	Cul1•Cand1•DCN1•Fb2•S2	0
Cul1•DCN1	0	N8-Cul1•Fb2	0	Cul1•Fb1•CSN	0
Cul1•CSN	0	N8-Cul1•Fb1•S1	0	Cul1•Fb2•CSN	0
S1 (IκBα-P)	0	N8-Cul1•Fb2•S2	0	Cul1•DCN1•CSN	0
S2 (auxiliary)	0	N8-Cul1•Fb1•CSN	0	Cul1•DCN1•Fb1•CSN	0
		N8-Cul1•Fb2•CSN	0	Cul1•DCN1•Fb2•CSN	0

[(a)] initial condition, [(b)] measured, [(c)] [FbT] = [Skp1], [(d)] β-TrCP, [(e)] [Fb2] = [FbT] - [Fb1], [(f)] auxiliary substrate receptors

F-box binding to Cul1

The assembly of a functional Skp1•Cul1•F-box (SCF) complex requires binding of a Skp1•F-box heterodimer to Cul1. Here, we did not model the formation of Skp1•F-box dimers explicitly, but considered them as preformed stable entities [Schulman et al., 2000]. In general, there are ~69 different SCF complexes in humans. In our model we considered only two types of Skp1•F-box proteins denoted by Fb1 and Fb2. This allows us to analyze the time scale for the degradation of a specific substrate (mediated by Fb1) in the presence of auxiliary substrate receptors (SRs). The latter compete with Fb1 for access to Cul1, and they are collectively denoted by Fb2.

In a previous study the assembly of ~50 F-box proteins with Cul1 has been quantified under different conditions [Reitsma et al., 2017]. Under normal conditions occupancy ranged from 0% to 70% indicating a highly non-equilibrium steady state *in vivo* that is driven by neddylation, F-box exchange and substrate availability. Even in the absence of neddylation occupancy ranged between 0% and 30% suggesting that there exists some variation in the expression level and/or the binding affinity of Cul1 for different F-box proteins. For the Skp1•Fbxw7 receptor biochemical studies yielded a dissociation constant of 0.225pM which increased by ~6 orders of magnitude to 650nM in the presence of Cand1 [Pierce et al., 2013]. This dramatic increase is mainly driven by a corresponding increase in the k_{off} while the k_{on} remained almost constant. In fact, modulating the off rate constant has been proposed as one of the main mechanisms through which cells may adjust their cellular SCF repertoire [Reitsma et al, 2017].

To allow β-TrCP (Fb1) to exhibit a different binding affinity from background SRs we fix k_{on} at the values obtained for Fbxw7 and express the off rate constants for Fb1 and Fb2 in terms of those for Fbxw7 as

$$k_{off,i}^{Fb1} = f_{Fb1} \cdot k_{off,i}^{Fbxw7} \quad \text{and} \quad k_{off,i}^{Fb2} = f_{Fb2} \cdot k_{off,i}^{Fbxw7}, \quad i = 1,2 \tag{S7}$$

where $k_{off,1}^{Fbxw7} = 9 \cdot 10^{-7} s^{-1}$ and $k_{off,2}^{Fbxw7} = 1.3 s^{-1}$ denote the off rate constants of Skp1•Fbxw7 from the binary and ternary complexes (involving Cand1), respectively [Pierce et al., 2013]. The values of the two scale parameters f_{Fb1} and f_{Fb2} were estimated by comparing model predictions with experiments (cf. Parameter estimation and Table T15).

Table T3

No.	Reactions involving Fb1	k_{on} [a] $[(M \cdot s)^{-1}]$	k_{off} $[s^{-1}]$
1	Cul1 + Fb1 ↔ Cul1•Fb1	$4 \cdot 10^6$	$f_{Fb1} \cdot 9 \cdot 10^{-7}$
1a	Cul1•DCN1 + Fb1 ↔ Cul1•DCN1•Fb1		
1b	Cul1 + Fb1•S1 ↔ Cul1•Fb1•S1		
1c	Cul1•DCN1 + Fb1•S1 ↔ Cul1•DCN1•Fb1•S1		
1d	N8-Cul1 + Fb1 ↔ N8-Cul1•Fb1		
1e	N8-Cul1 + Fb1•S1 ↔ N8-Cul1•Fb1•S1		
1f	N8-Cul1•CSN + Fb1 ↔ N8-Cul1•Fb1•CSN		
2	Cul1•Cand1 + Fb1 ↔ Cul1•Cand1•Fb1	$2 \cdot 10^6$	$f_{Fb1} \cdot 1.3$
2a	Cul1•Cand1•DCN1 + Fb1 ↔ Cul1•Cand1•DCN1•Fb1		
2b	Cul1•Cand1 + Fb1•S1 ↔ Cul1•Cand1•Fb1•S1		
2c	Cul1•Cand1•DCN1 + Fb1•S1 ↔ Cul1•Cand1•DCN1•Fb1•S1		

[a] measured for Skp1•Fbxw7 [Pierce et al., 2013]

Table T4

	Reactions involving Fb2	k_{on} $[(M \cdot s)^{-1}]$	k_{off} $[s^{-1}]$
	Cul1 + Fb2 ↔ Cul1•Fb2	$4 \cdot 10^6$	$f_{Fb2} \cdot 9 \cdot 10^{-7}$
	Cul1•DCN1 + Fb2 ↔ Cul1•DCN1•Fb2		
	Cul1 + Fb2•S2 ↔ Cul1•Fb2•S2		
	Cul1•DCN1 + Fb2•S2 ↔ Cul1•DCN1•Fb2•S2		
	N8-Cul1 + Fb2 ↔ N8-Cul1•Fb2		
	N8-Cul1 + Fb2•S2 ↔ N8-Cul1•Fb2•S2		
	N8-Cul1•CSN + Fb2 ↔ N8-Cul1•Fb2•CSN		
	Cul1•Cand1 + Fb2 ↔ Cul1•Cand1•Fb2	$2 \cdot 10^6$	$f_{Fb2} \cdot 1.3$
	Cul1•Cand1•DCN1 + Fb2 ↔ Cul1•Cand1•DCN1•Fb2		
	Cul1•Cand1 + Fb2•S2 ↔ Cul1•Cand1•Fb2•S2		
	Cul1•Cand1•DCN1 + Fb2•S2 ↔ Cul1•Cand1•DCN1•Fb2•S2		

As suggested by our experiments (Fig. 2H) we modeled the assembly of SCF complexes by a random-order binding mechanism (Fig. S4A), i.e. Skp1•F-box receptor proteins may first bind to Cul1 species and then bind substrate or vice versa. In fact, previous simulations indicated that an exchange factor becomes dispensable if binding occurs in a sequential order, i.e. if substrate only binds to F-box proteins if the latter are already bound to Cul1 [Straube et al., 2017].

Cand1 binding to Cul1

The exchange of Skp1•F-box proteins on Cul1 is catalyzed by Cand1 which acts as a substrate receptor exchange factor [Pierce et al., 2013]. Experiments suggest that Cand1 exerts its catalytic function similar to guanine nucleotide exchange factors (GEFs), i.e. through formation of a ternary (Cul1•Cand1•Fb) complex. In the absence of Skp1•F-box proteins spontaneous dissociation of Cand1 from a Cul1•Cand1 complex is extremely slow ($k_{off,3} = 10^{-5}s^{-1}$) but binding of Skp1•F-box to Cul1•Cand1 dramatically increases the dissociation constant for Cand1 in the ternary complex (reaction 4). On thermodynamic grounds (cf. Detailed balance relations) the increase of the dissociation constant for Cand1 upon binding of Skp1•F-box to Cul1•Cand1 must be the same as the increase of the dissociation constant for Skp1•F-box upon binding of Cand1 to Cul1•Skp1•F-box, i.e (cf. Fig. S4C)

$$\frac{K_2}{K_1} = \frac{K_4}{K_3} = \tau \tag{S8}$$

where $K_i = k_{off,i}/k_{on,i}$ denotes the dissociation constant of reaction i. Substituting the known values for K_1 $(0.225pM)$ and K_2 $(650nM)$ we obtain $\tau \approx 2.9 \cdot 10^6$ which is comparable with values obtained for the GEF-mediated GDP/GTP exchange [Goody & Hofmann-Goody, 2002].

To compute the remaining dissociation constants we measured the rate constants for the association between Cul1 and Cand1 ($k_{on,3}$) and that between Cul1•Skp1•Skp2 and Cand1 ($k_{on,4}$) (cf. Fig. 1). In this way we obtained $K_3 = 0.5pM$ and (using Eq. S8) $K_4 = (K_2/K_1)K_3 \approx 1.44\mu M$. The latter also determines the dissociation rate constant $k_{off,4}$ as

$$k_{off,4} = k_{on,4} \cdot (K_2/K_1) \cdot K_3 \approx 2.9s^{-1}.$$

Reactions 5 and 6 describe the binding of Cand1 to Cul1 when DCN1 is already bound to Cul1. Our pulldown assay with immobilized DCN1 on GST beads showed (Fig. 3C and 3D) that in the presence of Cand1 the K_D of DCN1 in the ternary Cul1•Cand1•DCN1 complex is reduced by a factor $\alpha = 1/36 = 0.0278$ (cf. Fig. S4C). To ensure that the K_D for Cand1 in the ternary complex is reduced by the same factor we multiplied the k_{off} for reaction 5 and 6 by α and kept k_{on} the same as for reactions 3 and 4 (Table T5).

Substrate binding to F-box protein

We assumed that substrate binds with equal affinity to free Skp1•F-box proteins as well as to Skp1•F-box proteins that are already bound to Cul1 (Cul1•Fb). In general, our model allows for two substrates that may differ in their binding parameters. In particular simulations S1 represents the phosphorylated form of IκBα (IκBα-P) while S2 plays the role of auxiliary (background) substrate which is always present in cells. The off rate constant ($k_{off} \sim 10^{-5}s^{-1}$) for the dissociation of IκBα-P from Cul1•β-TrCP•IκBα-P is very small (cf. Fig. S5E) comparable

to that for the dissociation of Skp1•F-box from an SCF complex. The on rate constant has not been measured, but is expected to lie between $10^6 - 10^7 (M \cdot s)^{-1}$. In the simulations we used the value $k_{on} = 10^7 (M \cdot s)^{-1}$ for both IκBα-P (S1) and auxiliary substrate (S2). Since the latter represents a mixture of different substrates (the type and amount of which is difficult to quantify for our experimental conditions) we assumed a less extreme value for the off rate constant of S2. The reactions involving S1 and S2 are listed in Table T6 and Table T7, respectively.

Table T5

No.	Reactions	$k_{on}\ [(M \cdot s)^{-1}]$	$k_{off}\ [s^{-1}]$
3	Cul1 + Cand1 ↔ Cul1•Cand1	$2 \cdot 10^7$ [(a)]	10^{-5} [(b)]
4	Cul1•Fb1 + Cand1 ↔ Cul1•Cand1•Fb1	$2 \cdot 10^6$ [(a)]	2.9 [(c)]
	Cul1•Fb2 + Cand1 ↔ Cul1•Cand1•Fb2		
4a	Cul1•Fb1•S1 + Cand1 ↔ Cul1•Cand1•Fb1•S1		
	Cul1•Fb2•S2 + Cand1 ↔ Cul1•Cand1•Fb2•S2		
5	Cul1•DCN1 + Cand1 ↔ Cul1•Cand1•DCN1	$2 \cdot 10^7$	$\alpha \cdot 10^{-5}$ [(d)]
6	Cul1•DCN1•Fb1 + Cand1 ↔ Cul1•Cand1•DCN1•Fb1	$2 \cdot 10^6$	$\alpha \cdot 2.9$
	Cul1•DCN1•Fb2 + Cand1 ↔ Cul1•Cand1•DCN1•Fb2		
6a	Cul1•DCN1•Fb1•S1 + Cand1 ↔ Cul1•Cand1•DCN1•Fb1•S1		
	Cul1•DCN1•Fb2•S2 + Cand1 ↔ Cul1•Cand1•DCN1•Fb2•S2		

[(a)] measured [(b)] measured [Pierce et al., 2013], [(c)] computed from Eq. (S8), [(d)] $\alpha = 0.0278$

Table T6

No.	Reactions involving S1	$k_{on}\ [(M \cdot s)^{-1}]$	$k_{off}\ [s^{-1}]$
7	Fb1 + S1 ↔ Fb1•S1	10^7 [(a)]	$3.3 \cdot 10^{-5}$ [(b)]
7a	Cul1•Fb1 + S1 ↔ Cul1•Fb1•S1		
7b	Cul1•Cand1•Fb1 + S1 ↔ Cul1•Cand1•Fb1•S1		
7c	Cul1•DCN1•Fb1 + S1 ↔ Cul1•DCN1•Fb1•S1		
7d	Cul1•Cand1•DCN1•Fb1 + S1 ↔ Cul1•Cand1•DCN1•Fb1•S1		
7e	N8-Cul1•Fb1 + S1 ↔ N8-Cul1•Fb1•S1		

[(a)] estimated, [(b)] measured

Table T7

No.	Reactions involving S2	$k_{on}\ [(M \cdot s)^{-1}]$	$k_{off}\ [s^{-1}]$
	Fb2 + S2 ↔ Fb1•S2	10^7 [(a)]	0.01 [(a)]
	Cul1•Fb2 + S2 ↔ Cul1•Fb2•S2		
	Cul1•Cand1•Fb2 + S2 ↔ Cul1•Cand1•Fb2•S2		
	Cul1•DCN1•Fb2 + S2 ↔ Cul1•DCN1•Fb2•S2		
	Cul1•Cand1•DCN1•Fb2 + S2 ↔ Cul1•Cand1•DCN1•Fb2•S2		
	N8-Cul1•Fb2 + S2 ↔ N8-Cul1•Fb2•S2		

[(a)] estimated

DCN1 binding to Cul1

DCN1 is a scaffold-like E3 ligase which is required for efficient Cul1 neddylation [Kurz et al., 2008]. Experiments have shown that DCN1 forms a stable ternary complex with Cul1 and Cand1 [Keuss et al., 2016]. In the absence of Cand1 the K_D for DCN1 binding to Cul1 is comparably low ($1.8\mu M$) [Monda et al., 2013] while binding of Cand1 increases the affinity of DCN1 to Cul1 36-fold (Fig. 3C and 3D), i.e. the K_D is lowered by a factor $\alpha = 1/36 = 0.0278$ (cf. Cand1 binding to Cul1). To generate a K_D of $1.8\mu M$ we set $k_{on} = 10^6\ (M \cdot s)^{-1}$ and $k_{off} = 1.8\ s^{-1}$ (Table T8). When Cand1 is bound to Cul1 we keep k_{on}, but lower k_{off} by a factor α.

Table T8

No.	Reactions	$k_{on}\ [(M \cdot s)^{-1}]$	$k_{off}\ [s^{-1}]$
8	Cul1 + DCN1 ↔ Cul1•DCN1	10^6 [(a)]	1.8 [(b)]
8a	Cul1•Fb1 + DCN1 ↔ Cul1•DCN1•Fb1		
	Cul1•Fb2 + DCN1 ↔ Cul1•DCN1•Fb2		
8b	Cul1•Fb1•S1 + DCN1 ↔ Cul1•DCN1•Fb1•S1		
	Cul1•Fb2•S2 + DCN1 ↔ Cul1•DCN1•Fb2•S2		
9	Cul1•Cand1 + DCN1 ↔ Cul1•Cand1•DCN1	10^6	$\alpha \cdot 1.8$ [(c)]
9a	Cul1•Cand1•Fb1 + DCN1 ↔ Cul1•Cand1•DCN1•Fb1		
	Cul1•Cand1•Fb2 + DCN1 ↔ Cul1•Cand1•DCN1•Fb2		
9b	Cul1•Cand1•Fb1•S1 + DCN1 ↔ Cul1•Cand1•DCN1•Fb1•S1		
	Cul1•Cand1•Fb2•S2 + DCN1 ↔ Cul1•Cand1•DCN1•Fb2•S2		

[(a)] estimated, [(b)] adjusted so that $K_D = 1.8\mu M$ [Monda et al., 2013], [(c)] $\alpha = 0.0278$

Detailed balance relations

The CRL network contains several thermodynamic cycles two of which are depicted in Fig. S4C. Since each of these cycles comprises only of reversible equilibria there must be no net flux in each cycle at steady state. In physical terms, this means that the change in free energy for the formation of the ternary complexes (Cul1•Cand1•Fb and Cul1•Cand1•DCN1) must not depend on the order in which they are formed. This constraint leads to detailed balance relations between the dissociation constants in each cycle, i.e. $K_1 \cdot K_4 = K_2 \cdot K_3$ and $K_3 \cdot K_9 = K_5 \cdot K_8$. A similar relation also holds for the cycle comprising the reactions 4, 6, 8a, and 9a which leads to $K_4 \cdot K_9 = K_8 \cdot K_6$.

Neddylation reactions

Since DCN1 is required for efficient neddylation of Cul1 [Kurz et al., 2008] and since Cand1 binding and N8 conjugation cannot occur simultaneously [Liu et al., 2002] we assumed that neddylation can only occur from SCF states where DCN1 is bound to Cul1 *and* Cand1 is not bound to Cul1. In general, Nedd8 (N8) conjugation is catalyzed by an associated E2 enzyme (e.g. UBC12) which is recruited to the Rbx1 domain of an SCF complex. However, the rate constants for E2 binding and N8 conjugation are not known. To keep the number of unknown parameters as small as possible we model neddylation by a first order process (Table T9) with effective neddylation rate constant k_{nedd} which is treated as a variable parameter to be estimated from experiments (cf. Table T15). Also, since the concentration of N8 is much larger

than that of the other proteins (cf. Table T1) we assumed that N8 is not limiting for the reaction so that it can be absorbed into the definition of the rate constant.

Table T9

No.	Reactions	$k_{nedd}\ [s^{-1}]$
10	Cul1•DCN1 → N8-Cul1 + DCN1	0.268 [(a)]
10a	Cul1•DCN1•Fb1 → N8-Cul1•Fb1 + DCN1	
	Cul1•DCN1•Fb2 → N8-Cul1•Fb2 + DCN1	
10b	Cul1•DCN1•Fb1•S1 → N8-Cul1•Fb1•S1 + DCN1	
	Cul1•DCN1•Fb2•S2 → N8-Cul1•Fb2•S2 + DCN1	

[(a)] estimated

Deneddylation reactions

Deneddylation is mediated by the COP9 signalosome (CSN). Consistent with measurements of the rate constants for CSN-mediated deneddylation of N8-Cul1 [Mosadeghi et al., 2016] we assumed that CSN first binds reversibly to N8-Cul1 and N8-Cul1•Fb (11 and 11a) and, in a second step, N8 is cleaved leading to the dissociation of CSN (12 and 12a).

Table T10

No.	Reactions	$k_{on}\ [(M \cdot s)^{-1}]$	$k_{off}\ [s^{-1}]$	$k_{cat}\ [s^{-1}]$
11	N8-Cul1 + CSN ↔ N8-Cul1•CSN	$2 \cdot 10^7$ [(a)]	0.032 [(a)]	
11a	N8-Cul1•Fb1 + CSN ↔ N8-Cul1•Fb1•CSN			
	N8-Cul1•Fb2 + CSN ↔ N8-Cul1•Fb2•CSN			
12	N8-Cul1•CSN → Cul1 + CSN			1.1 [(a)]
12a	N8-Cul1•Fb1•CSN → Cul1•Fb1 + CSN			
	N8-Cul1•Fb2•CSN → Cul1•Fb2 + CSN			

[(a)] measured [Mosadeghi et al., 2016]

Product inhibition of CSN

While neddylated Cul1 is a substrate of the CSN deneddylated Cul1 acts as an inhibitor of CSN activity [Mosadeghi et al., 2016]. CSN binds to both neddylated and deneddylated Cul1, but with different binding affinity. While the k_{on} is the same for both reactions the k_{off} for CSN in complex with non-neddylated Cul1 is increased by a factor of ~200. Previous biochemical analysis has shown that, in the presence of Cand1 or substrate, the deneddylation rate is reduced [Emberley et al., 2012]. Moreover, addition of substrate impedes stable association of CSN with SCF [Enchev et al., 2012]. Hence, to model product inhibition of CSN we assumed that CSN only binds to Cul1, Cul1•Fb, Cul1•DCN1 and Cul1•DCN1•Fb states (cf. Table T11).

Table T11

No.	Reactions	$k_{on}\ [(M \cdot s)^{-1}]$	$k_{off}\ [s^{-1}]$
13	Cul1 + CSN ↔ Cul1•CSN	$2 \cdot 10^7$ [(a)]	6.2 [(a)]
13a	Cul1•Fb1 + CSN ↔ Cul1•Fb1•CSN		
	Cul1•Fb2 + CSN ↔ Cul1•Fb2•CSN		
13b	Cul1•DCN1 + CSN ↔ Cul1•DCN1•CSN		
13c	Cul1•DCN1•Fb1 + CSN ↔ Cul1•DCN1•Fb1•CSN		
	Cul1•DCN1•Fb2 + CSN ↔ Cul1•DCN1•Fb2•CSN		

[(a)] measured [Mosadeghi et al., 2016]

Substrate degradation

Substrate degradation by itself is a complex process which involves recruitment of Ub-loaded E2 enzyme to the Rbx1 domain of an SCF complex, subsequent multiple Ub transfers to the substrate and processing by the 26S proteasome. Here, we neglected much of this complexity and assumed that once a substrate-bound SCF complex is neddylated the substrate can be degraded. The latter process was described by first order rate constant k_{deg} which summarizes the above mentioned processes in an effective manner (Table T12). Also, for simplicity we assumed that the degradation rate constant is the same for S1 (IκBα-P) and background substrate S2. For the human 26S proteasome substrate degradation rates range from less than $0.01\ min^{-1}$ up to $0.7\ min^{-1}$ depending on the substrate and the number of conjugated ubiquitins [Lu et al., 2016]. For CyclinB-NT with 4 conjugated ubiquitins the degradation rate is $0.5\ min^{-1}$ or $0.0083\ s^{-1}$. Based on our measurements we estimated $k_{deg} = 0.0071\ s^{-1}$ (cf. Table T15).

Table T12

No.	Reactions	$k_{deg}\ [s^{-1}]$
14	N8-Cul1•Fb1•S1 → N8-Cul1•Fb1	0.0071 [(a)]
	N8-Cul1•Fb2•S2 → N8-Cul1•Fb2	

[(a)] estimated

Background substrate

To generate the high degree of Cul1 neddylation observed experimentally we had to assume that cells contain a certain amount of CRL substrates, which is consistent with the fact that substrate favors the neddylated state of CRL ligases [Emberley et al., 2012; Enchev et al., 2012]. To generate auxiliary substrate we assumed a constitutive synthesis term (Table T13). Since the total amount of background CRL substrates in the cell is unknown we treated the synthesis rate as a variable parameter to be determined by comparison with experiments (cf. Table T15). In this way we obtained an estimate of 2261nM for the concentration of background substrate under steady state conditions in wildtype cells assuming that substrates are only degraded via the CRL-mediated pathway.

Table T13

No.	reaction	$k_{synth}^{S2}\ [nM \cdot s^{-1}]$
15	Ø → S2	1.4 [(a)]

[(a)] estimated

Simulations were done with the Systems Biology Toolbox of MATLAB [MATLAB 2015b] which was used to translate the model reactions (1-15) into a system of ordinary differential equations using mass-action kinetics. Integrations were performed with the implicit solver *ode15s*.

Parameter estimation

To validate our model we measured different quantities in wildtype (WT) cells as well as in response to different genetic perturbations (cf. Table T14). Conditions listed in **bold font** were used to estimate the values of unknown parameters. Altogether, our model comprises 54 state variables and 35 parameters (rate constants, protein concentrations and scale parameters) from which 22 parameters were either known from previous experiments or measured in this work. Among the 13 remaining parameters 8 parameters could be reasonably estimated or constrained leaving only 5 parameters to be fitted by comparing model simulations with experiments. The 4 scale factors P1 – P4 (Table T15) were estimated based on relative protein abundances and previous measurements of the association of Cand1 with different cullins. The 4 on and off rate constants P5 – P8 had almost no effect on the value of the measured quantities (cf. T14 and Fig. S5B), so we fixed them at the indicated values to reduce the number of variable parameters during the fitting procedure.

Table T14 – Experimental conditions and measured quantities

measured quantity	**cell type / perturbation / condition**	**type of experiment**	**figure**
Cul1.b2.Cand1[(a)]	**WT**[(e)] / WT + MLN4924	steady state	4B
Cul1.b2.Skp1[(b)]	WT / WT + MLN4924 / DKO[(f)]	steady state	4B
Cul1.b2.N8[(c)]	**WT** / WT + Cul1 / **DKO** / DKO + Cul1	steady state	4E
β-TrCP.b2.Cul1[(d)]	**WT**	steady state	4D
$t_{1/2}$	**WT** / **DKO** / DKO + Cand1	transient	4C
	WT + β-TrCP / WT + Cul1 / DKO + β-TrCP / DKO + Cul1		4F

[(a)] fraction of Cul1 bound to Cand1, [(b)] fraction of Cul1 bound to Skp1, [(c)] fraction of Cul1 bound to Nedd8, [(d)] fraction of β-TrCP bound to Cul1, [(e)] WT – wildtype, [(f)] DKO – double knockout Cand1$^{-/-}$, Cand2$^{-/-}$

To estimate the values of the 5 remaining parameters in Table T15 (P9-P13) we used nonlinear optimization in combination with a profile likelihood approach as described in [Raue et al., 2009]. To calibrate the model we defined the weighted sum of squared residuals as an objective function

$$\chi^2(\theta) := \sum_{k=1}^{6} \frac{\left(y_k - y_k(\theta)\right)^2}{\sigma_k^2} \tag{S9}$$

and numerically determined $\theta = \left(f_{Fb1}, f_{Fb2}, k_{nedd}, k_{deg}, k_{synth}^{S2}\right)$ such that

$$\hat{\theta} = \operatorname{argmin}\left[\chi^2(\theta)\right].$$

In Eq. (S9) y_k and σ_k^2 denote the values of the measured quantities (cf. T14, bold face) and their respective measurement errors. The quantities $y_k(\theta)$ are the predicted values of the measured quantities obtained from numerical simulations of our model for a particular set of parameter values. Due to limited sample size we were not able to reliably estimate the measurement errors from the data. So, for convenience, we assumed equal variances of

$\sigma_k^2 = 0.1 y_k$ (10% from the mean values) for all measurements. However, since all parameters are identifiable (see below) a different choice for the values of the variances would yield qualitatively similar results.

To obtain confidence intervals for the estimated parameter values we numerically computed the profile likelihood for each parameter defined as

$$\chi^2_{PL}(\theta_i) = \min_{\theta_{j\neq i}}[\chi^2(\theta)], \tag{S10}$$

i.e. for each value of θ_i the objective function defined in Eq. (S9) was re-optimized with respect to the remaining parameters $\theta_{j\neq i}$. The resulting plots exhibit a parabolic shape (Fig. S5A) indicating that all parameters are identifiable [Raue et al., 2009]. To obtain finite sample confidence intervals we defined the confidence regions

$$\{\theta_i : \chi^2_{PL}(\theta) - \chi^2(\hat{\theta}) < \Delta_\alpha\}, \qquad i = 1, \ldots, 5 \tag{S11}$$

where the threshold $\Delta_\alpha = \chi^2(\alpha, df)$ is the α quantile (confidence level) of the χ^2-distribution with df degrees of freedom. Pointwise confidence intervals are obtained for $df = 1$ while $df = 5$ yields simultaneous confidence intervals for all 5 parameters. Confidence intervals for model predictions (cf. Fig. 4) were computed by running simulations for parameters sampled from the confidence region defined by Eq. (S11) with the threshold $\Delta_\alpha = \chi^2(0.95,5)$ (Fig. S5A, upper horizontal line).

Table T15 – List of estimated parameters

parameter		value	expected range	defined in	fixed / variable
P1	f_{DCN1}	6	$5 - 6$	Eq. (S1)	fixed
P2 P3	$f_{DCN1,WT}$ $f_{CSN,WT}$	0.23		Eqs. (S2) – (S4)	fixed
P4	$f_{Cand1,WT}$	0.54			fixed
P5	k_{on}^{S1}	$10^7\ (Ms)^{-1}$	$10^6 - 10^7\ (Ms)^{-1}$	Table T6	fixed
P6	k_{on}^{S2}	$10^7\ (Ms)^{-1}$	$10^6 - 10^7\ (Ms)^{-1}$	Table T7	fixed
P7	k_{off}^{S2}	$0.01 s^{-1}$	$0.0001 - 0.01\ s^{-1}$	Table T7	fixed
P8	k_{on}^{DCN1}	$10^6\ (Ms)^{-1}$	$10^6 - 10^7\ (Ms)^{-1}$	Table T8	fixed
P9	f_{Fb1}	0.247	$0.102 - 0.490$ [(a)]	Eq. (S7)	variable
P10	f_{Fb2}	6.514	$2.978 - 17.461$ [(a)]	Eq. (S7)	variable
P11	k_{nedd}	$0.268\ s^{-1}$	$0.134\ - 0.626\ s^{-1}$ [(a)]	Table T9	variable
P12	k_{deg}	$0.0071\ s^{-1}$	$0.0055 - 0.0091\ s^{-1}$ [(a)]	Table T12	variable
P13	k_{synth}^{S2}	$1.40\ nM \cdot s^{-1}$	$1.09 - 1.85\ nM \cdot s^{-1}$ [(a)]	Table T13	variable

[(a)] simultaneous confidence intervals to a 95% confidence level with 10% assumed measurement errors.

Response coefficients

To quantify how small changes in one of the parameters (P5 – P13) would impact the predicted values for the measured quantities (cf. T14) we computed the matrix of response coefficients (Fig. S5B) according to

$$R_{ij} \coloneqq \frac{\Delta Q_i / Q_i^{ref}}{\Delta P_j / P_j^{ref}} \tag{S12}$$

where $\Delta P_j = P_j - P_j^{ref}$ denotes the change of parameter P_j relative to a reference value P_j^{ref} and $\Delta Q_i = Q_i - Q_i^{ref}$ represents the corresponding change of the predicted quantity Q_i. Depending on whether Q_i increases or decreases upon a parameter change ΔP_j the response coefficient R_{ij} may be positive or negative, respectively. Its magnitude quantifies the fractional change of Q_i upon a fractional change of P_j. The fact that almost all response coefficients satisfy $|R_{ij}| < 1$ means that our system exhibits only a weak sensitivity to most of the parameters at the respective reference point. This is particularly true for the 4 on and off rate constants P5 – P8 which have almost no effect on the predicted values of the measured quantities except for k_{on}^{DCN} which weakly affects the half-life for substrate degradation in DKO cells. To reduce the number of fitting parameters we have, therefore, fixed P5 – P8 during parameter estimation.

From the entries of the response matrix for the remaining parameters (P9 – P13) we can make some interesting observations: The fractions of Cul1 bound to Cand1, Skp1 and Nedd8 (first three rows) are mainly determined by the ratio between substrate synthesis (k_{synth}^{S2}) and degradation (k_{deg}). If the substrate synthesis rate is increased the neddylated fraction of Cul1 increases and more Skp1•F-box proteins are recruited to Cul1 leading to a reduction of the fraction of Cul1 associated with Cand1. Increasing k_{deg} has the opposite effect. However, the latter also affects the half-life for IκBα degradation while k_{synth}^{S2} has only a minor effect on $t_{1/2}$. Interestingly the total concentration of Skp1•F-box proteins (FbT) has a strong positive effect on the half-life for IκBα degradation in DKO cells because increasing the total pool of F-box proteins reduces the amount of Cul1 available for binding to β-TrCP.

Protein fractions in terms of state variables

To relate the measured quantities defined in Table T14 to state variables in our model (cf. Table 2) we used the following relations: The fraction of Cul1 bound to Nedd8 was computed as

$$\begin{aligned}\mathrm{Cul1.b2.N8} = {} & \frac{[\mathrm{N8\text{-}Cul1}] + [\mathrm{N8\text{-}Cul1 \bullet Fb1}] + [\mathrm{N8\text{-}Cul1 \bullet Fb2}]}{\mathrm{Cul1_T}} \\ & + \frac{[\mathrm{N8\text{-}Cul1 \bullet Fb1 \bullet S1}] + [\mathrm{N8\text{-}Cul1 \bullet Fb2 \bullet S2}] + [\mathrm{N8\text{-}Cul1 \bullet CSN}]}{\mathrm{Cul1_T}} \\ & + \frac{[\mathrm{N8\text{-}Cul1 \bullet Fb1 \bullet CSN}] + [\mathrm{N8\text{-}Cul1 \bullet Fb2 \bullet CSN}]}{\mathrm{Cul1_T}}\end{aligned}$$

where $Cul1_T$ denotes the total concentration of Cul1 defined in Table T1. To define the fractions of Cul1 bound to Cand1 (Cul1.b2.Cand1) and Cul1 bound to Skp1•F-box (Cul1.b2.Skp1) we had to take into account that higher-order complexes involving Cand1 and Fb1 or Fb2 are unstable and, thus, cannot be detected in our pull-down assays. For example, the complexes Cul1•Cand1•Fbi•Si would rapidly decay into Cul1•Fbi•Si and Cand1 or Cul1•Cand1 and Fbi•Si (Fig. S5C). The corresponding probabilities are given by

$$a_i = \frac{k_{off,2}^{Si}}{k_{off,2}^{Si} + k_{off,4}} \quad \text{and} \quad b_i = 1 - a_i = \frac{k_{off,4}}{k_{off,2}^{Si} + k_{off,4}}, \quad i = 1,2 \tag{S13}$$

where the rate constants $k_{off,2}^{Si}$ and $k_{off,4}$ are defined in Tables T3-T5. For the decay of complexes involving Cand1, DCN1 and Fb1 or Fb2 we considered three decay channels as the dissociation of Cand1 and DCN1 from Cul1•Cand1•DCN1•Fbi•Si or Cul1•Cand1•DCN1•Fbi occurs with similar rates. The respective probabilities are given by

$$c_i = \frac{k_{off,2}^{Si}}{k_{off,2}^{Si} + k_{off,6} + k_{off,9}}, \quad d_i = \frac{k_{off,6}}{k_{off,2}^{Si} + k_{off,6} + k_{off,9}}, \quad e_i = 1 - (c_i + d_i), \tag{S14}$$

for $i = 1,2$ where the rate constants $k_{off,6}$ and $k_{off,9}$ are defined in Tables T5 and T8, respectively. With the help of these probabilities the protein fractions Cul1.b2.Cand1 and Cul1.b2.Skp1 (which we set equal to Cul1.b2.Fb1+Cul1.b2.Fb2) are defined by

$$\begin{aligned}\mathrm{Cul1.b2.Cand1} = {} & \frac{[\mathrm{Cul1 \bullet Cand1}] + a_1([\mathrm{Cul1 \bullet Cand1 \bullet Fb1}] + [\mathrm{Cul1 \bullet Cand1 \bullet Fb1 \bullet S1}])}{\mathrm{Cul1_T}} \\ & + \frac{a_2([\mathrm{Cul1 \bullet Cand1 \bullet Fb2}] + [\mathrm{Cul1 \bullet Cand1 \bullet Fb2 \bullet S2}]) + [\mathrm{Cul1 \bullet Cand1 \bullet DCN1}]}{\mathrm{Cul1_T}} \\ & + \frac{(a_1 e_1 + c_1)([\mathrm{Cul1 \bullet Cand1 \bullet DCN1 \bullet Fb1}] + [\mathrm{Cul1 \bullet Cand1 \bullet DCN1 \bullet Fb1 \bullet S1}])}{\mathrm{Cul1_T}} \\ & + \frac{(a_2 e_2 + c_2)([\mathrm{Cul1 \bullet Cand1 \bullet DCN1 \bullet Fb2}] + [\mathrm{Cul1 \bullet Cand1 \bullet DCN1 \bullet Fb2 \bullet S2}])}{\mathrm{Cul1_T}}\end{aligned}$$

and

$$\begin{aligned}\mathrm{Cul1.b2.Fbi} = {} & \frac{[\mathrm{Cul1 \bullet Fbi}] + [\mathrm{Cul1 \bullet Fbi \bullet Si}] + [\mathrm{Cul1 \bullet DCN1 \bullet Fbi}]}{\mathrm{Cul1_T}} \\ & + \frac{b_i([\mathrm{Cul1 \bullet Cand1 \bullet Fbi}] + [\mathrm{Cul1 \bullet Cand1 \bullet Fbi \bullet Si}])}{\mathrm{Cul1_T}} \\ & + \frac{(b_i e_i + d_i)([\mathrm{Cul1 \bullet Cand1 \bullet DCN1 \bullet Fbi}] + [\mathrm{Cul1 \bullet Cand1 \bullet DCN1 \bullet Fbi \bullet Si}])}{\mathrm{Cul1_T}} \\ & + \frac{[\mathrm{N8\text{-}Cul1 \bullet Fbi}] + [\mathrm{N8\text{-}Cul1 \bullet Fbi \bullet Si}] + [\mathrm{N8\text{-}Cul1 \bullet Fbi \bullet CSN}]}{\mathrm{Cul1_T}} \\ & + \frac{[\mathrm{Cul1 \bullet DCN1 \bullet Fbi \bullet CSN}] + [\mathrm{Cul1 \bullet Fbi \bullet CSN}] + [\mathrm{Cul1 \bullet DCN1 \bullet Fbi \bullet Si}]}{\mathrm{Cul1_T}}\end{aligned}$$

for $i = 1,2$. The fraction of β-TrCP bound to Cul1 (β-TrCP.b2.Cul1) is given by

$$\beta\text{-TrCP.b2.Cul1} = \mathrm{Cul1.b2.Fb1}\,\frac{\mathrm{Cul1_T}}{\mathrm{Fb1_T}}$$

where $\mathrm{Fb1_T}$ equals the total β-TrCP concentration listed in Table T1.

Simulation protocols

To simulate IκBα degradation of we started simulations from steady state by adding the reaction

No.	reaction	$k_{phos}\ [s^{-1}]$	initial condition
16	IκBα → IκBα-P (S1)	$\ln(2)/(60 \cdot 14)$	[IκBα]=647nM

which describes the phosphorylation of IκBα by IκBα kinase. Phosphorylated IκBα (IκBα-P) is generated with a half-life of 14min serving as a substrate of the $SCF^{\beta\text{-TrCP}}$ ligase ($\mathrm{Cul1} \bullet \mathrm{Fb1}$).

To simulate the conditions and perturbations listed in Table T14 we used the protocols defined in Table T16. Inhibition of Nedd8 conjugation as well as $Cand1^{-/-}$, $Cand2^{-/-}$ double knockout were simulated by setting the neddylation rate constant and the total Cand1 concentration to zero, respectively. To simulate Cul1 overexpression we computed a scale factor assuming that Cul1 competes with other cullins for access to Rbx1. Similarly, to simulate β-TrCP overexpression we computed a scale factor assuming that β-TrCP competes with auxiliary SRs for access to Skp1. In the case of Cul1 overexpression we also had to recompute the scale factors that account for sequestration of DCN1, CSN and Cand1 by other cullins. In both cases the overexpression factors (f_{Cul1} and $f_{\beta\text{-TrCP}}$) account for both endogenous and exogenous proteins.

Table T16

perturbation	protocol	remark
WT + MLN4924	set $k_{nedd} = 0$ at $t = 0$	Inhibition of Nedd8 conjugation
DKO	set $[Cand1] = 0$ at $t = 0$	$Cand1^{-/-}$, $Cand2^{-/-}$ double knockout
WT / DKO + Cul1	set $[Cul1]_{OE} = f_{OE,Cul1} \cdot [Cul1]_{WT}$ [(a)] with $f_{OE,Cul1}$ [(b)] $= \frac{f_{Cul1}[Rbx1]}{[Rbx1] + (f_{Cul1} - 1)[Cul1]_{WT}}$ and recompute scale factors in Eqs. (S2) – (S4) $f_{DCN1,OE}$ [(c)] $= \frac{[Cul1]_{OE}}{[Cul1]_{OE} + [Rbx1] - [Cul1]_{WT} + [Cul5]}$ $f_{Cand1,OE}$ [(d)] $= min\left(1, f_{Cand1,WT}\frac{f_{DCN1,OE}}{f_{DCN1,WT}}\right)$	Cul1 overexpression in WT or DKO
WT / DKO + β-TrCP	set $[Fb1]_{OE} = f_{OE,\beta\text{-TrCP}} \cdot [Fb1]_{WT}$ [(e)] with $f_{OE,\beta\text{-TrCP}}$ [(f)] $= \frac{f_{\beta\text{-TrCP}}[FbT]_{WT}}{[FbT]_{WT} + (f_{\beta\text{-TrCP}} - 1)[Fb1]_{WT}}$ set $[FbT]_{OE} = [FbT]_{WT} - [Fb1]_{OE}$	β-TrCP overexpression in WT or DKO

[(a)] $[Cul1]_{WT} = 522nM$, [(b)] $f_{Cul1} = 6.6$ in WT and $f_{Cul1} = 5$ in DKO, [(c)] $f_{CSN,OE} = f_{DCN1,OE}$, [(d)] not applicable in DKO, [(e)] $[Fb1]_{WT} = 64nM$, [(f)] $f_{\beta\text{-TrCP}} = 5.5$ in WT and $f_{\beta\text{-TrCP}} = 8$ in DKO, $[FbT]_{WT} = 2107nM$

Computation of the cycle time

To compute the cycle time for the cyclic reaction chain depicted in Fig. 7 we assigned to each reversible reaction an effective forward rate constant using the concept of net rate constants [Cleland, 1975]. The latter are denoted by $k_1,\ldots,k_6$ in Fig. S5D (highlighted in red color). For irreversible reactions such as neddylation (k_{10}) and deneddylation (k_{12}) the net rate constant is identical with the rate constant. Then the net rate constant k_6 is given by

$$k_6 = k_{on,11}[CSN]\frac{k_{12}}{k_{12} + k_{off,11}} \quad \text{(S15)}$$

where $[CSN] = 82nM$ denotes the concentration of free (unbound) CSN under steady state conditions (with [S1]=0). The other 5 net rate constants are defined recursively as

$$k_5 = k_{off,6}\frac{k_{10}}{k_{10} + k_{on,6}[Cand1]} \quad \text{(S16)}$$

$$k_4 = k_{on,2}([Fb1] + [Fb2] + [Fb2 \bullet S2])\frac{k_5}{k_5 + k_{off,2}} \quad \text{(S17)}$$

$$k_3 = k_{on,9}[DCN1]\frac{k_4}{k_4 + k_{off,9}} \quad \text{(S18)}$$

$$k_2 = k_{off,2}\frac{k_3}{k_3 + k_{on,2}[Fb1]} \quad \text{(S19)}$$

$$k_1 = k_{on,4}[Cand1]\frac{k_2}{k_2 + k_{off,4}}. \quad \text{(S20)}$$

The concentrations for Cand1, Fb1 (β-TrCP), Fb2 (auxiliary SR), Fb2•S2 and DCN1 are steady state concentrations that were obtained by integrating the model equations using the parameter set for WT cells (Tables T2-T13, T15) without substrate for Fb1. Note that in Eq. (S14) the factor in front of the fraction represents the effective “on rate” for binding of any free Skp1•F-box protein to Cul1•Cand1•DCN1 while in Eq. (S16) we used the on rate for binding of a particular F-box protein (Fb1) to bind to Cul1•Cand1. Combining the expressions in Eq. (S15) – (S20) yields the estimate for the average cycle time

$$t_{cycle} = \frac{1}{k_1} + \frac{1}{k_2} + \frac{1}{k_3} + \frac{1}{k_4} + \frac{1}{k_5} + \frac{1}{k_6} + \frac{1}{k_{10}} + \frac{1}{k_{12}}. \quad \text{(S21)}$$

Supplemental References

Cleland, W.W. (1975). Partition analysis and the concept of net rate constants as tools in enzyme kinetics. Biochemistry 14, 3220–3224.

Emberley, E.D., Mosadeghi, R., and Deshaies, R.J. (2012). Deconjugation of Nedd8 from Cul1 is directly regulated by Skp1-F-box and substrate, and the COP9 signalosome inhibits deneddylated SCF by a noncatalytic mechanism. J. Biol. Chem. 287, 29679–29689.

Enchev, R.I., Scott, D.C., da Fonseca, P.C., Schreiber, A., Monda, J.K., Schulman, B.A., Peter, M., and Morris, E.P. (2012). Structural basis for a reciprocal regulation between SCF and CSN. Cell Rep. 2, 616–627.

Keuss, M.J., Thomas, Y., Mcarthur, R., Wood, N.T., Knebel, A., and Kurz, T. (2016). Characterization of the mammalian family of DCN-type NEDD8 E3 ligases. J. Cell Sci. 129, 1441–1454.

Kulak, N.A., Pichler, G., Paron, I., Nagaraj, N., and Mann, M. (2014). Minimal, encapsulated proteomic-sample processing applied to copy-number estimation in eukaryotic cells. Nat. Methods 11, 319–324.

Kurz, T., Chou, Y.C., Willems, A.R., Meyer-Schaller, N., Hecht, M.L., Tyers, M., Peter, M., and Sicheri, F. (2008). Dcn1 functions as a scaffold-type E3 ligase for cullin neddylation. Mol. Cell 29, 23–35.

Liu, J., Furukawa, M., Matsumoto, T., and Xiong, Y. (2002). NEDD8 modification of CUL1 dissociates p120(CAND1), an inhibitor of CUL1-SKP1 binding and SCF ligases. Mol. Cell 10, 1511–1518.

Lu, Y., Lee, B.H., King, R.W., Finley, D., and Kirschner, M.W. (2015). Substrate degradation by the proteasome: a single-molecule kinetic analysis. Science 348, 1250834.

Raue, A., Kreutz, C., Maiwald, T., Bachmann, J., Schilling, M., Klingmüller, U., and Timmer, J. (2009). Structural and practical identifiability analysis of partially observed dynamical models by exploiting the profile likelihood. Bioinformatics 25, 1923–1929.

Schulman, B.A., Carrano, A.C., Jeffrey, P.D., Bowen, Z., Kinnucan, E.R.E., Finnin, M.S., Elledge, S.J., Harper, J.W., Pagano, M., and Pavletich, N.P. (2000). Insights into SCF ubiquitin ligases from the structure of the Skp1-Skp2 complex. Nature 408, 381–386.